Chicxulub and Popigai

after 15 years*

double or multiple impact craters?

* Klokočník J., Kostelecký J., Pešek I., Novák P., Wagner C.A., Sebera J. 2010. Candidates for multiple impact craters?: Popigai and Chicxulub as seen by the global high resolution gravitational field model EGM08, *Solid Earth EGU* **1**, 71-83; DOI: 10.5194/se-1-71-2010. See also: Is Chicxulub a double impact crater? *6th EGU A. von Humboldt Interntl. Conf. on Climate Change, Natural Hazards, and Societies*, Mérida, México, Section: The Cretaceous/Tertiary Boundary and the Chicxulub Impact Crater, paper AvH6-5, 15 March 2010.

Astronomical Institute of the Czech Academy of Sciences

Supplement 2
Tutorial

© ASU & RIGTC

Gravitational aspects (descriptors)

Gravity aspect	Explanation
T	Disturbing static gravitational potential
Δg	Gravity anomaly or perturbation (various versions)
Γ	Marussi tensor (just 5 independent second derivatives of T)
T_{zz}	Element of the Marussi tensor (second derivative of T in the radial direction), usually most important
I_j	3 gravity invariants of the Γ (I_0, I_1, I_2); preserved under any coordinate rotation
I	a ratio of I_1, I_2; when I~0, the causative body is ~2D; when $I \rightarrow 1$, causative body is 3D
θ	Strike angle is the main direction of Γ, under certain conditions
vd	Virtual deformation based on horizontal derivatives of T in latitudinal and longitudinal directions, expressing dilatation and pure sheer (compression)

Disturbing static gravitational potential outside the Earth masses in spherical harmonic expansion

$$T(r,\varphi,\lambda) = \frac{GM}{r}\sum_{l=2}^{\infty}\sum_{m=0}^{l}\left(\frac{R}{r}\right)^{l}\left(C'_{l,m}\cos m\lambda + S_{l,m}\sin m\lambda\right) P_{l,m}(\sin\varphi)$$

where *GM* is a product of the universal gravitational constant and the mass of the Earth (also known as the geocentric gravitational constant), *r* is the radial distance of an external point where *T* is computed, *R* is the radius of the Earth (which can be approximated by the semi-major axis of a reference ellipsoid), $P_{l,m}(\sin\varphi)$ are the Legendre associated functions, *l* and *m* are the degree and order of the harmonic expansion, (φ, λ) are the geocentric latitude and longitude, $C'_{l,m}$ and $S_{l,m}$ are the harmonic geopotential coefficients (Stokes parameters), fully normalized, $C'_{l,m} = C_{l,m} - C^{el}_{l,m}$, where $C^{el}_{l,m}$ belongs to the reference ellipsoid.

The spherical approximation of the *gravity anomaly* Δg is computed

$$\Delta g = -\frac{\partial T}{\partial r} - 2\frac{T}{r}$$

or one can use the *gravity disturbance* (it is the same but without the second term).

Gravity gradient tensor **Γ** (the Marussi tensor) is a tensor of the second derivatives of the disturbing potential *T:*

$$\mathbf{\Gamma} = \begin{bmatrix} T_{xx} & T_{xy} & T_{xz} \\ T_{yx} & T_{yy} & T_{yz} \\ T_{zx} & T_{zy} & T_{zz} \end{bmatrix} = \begin{bmatrix} \frac{\partial^2 V}{\partial x^2} & \frac{\partial^2 V}{\partial x \partial y} & \frac{\partial^2 V}{\partial x \partial z} \\ \frac{\partial^2 V}{\partial y \partial x} & \frac{\partial^2 V}{\partial y^2} & \frac{\partial^2 V}{\partial y \partial z} \\ \frac{\partial^2 V}{\partial z \partial x} & \frac{\partial^2 V}{\partial z \partial y} & \frac{\partial^2 V}{\partial z^2} \end{bmatrix} \qquad \textbf{(2)}$$

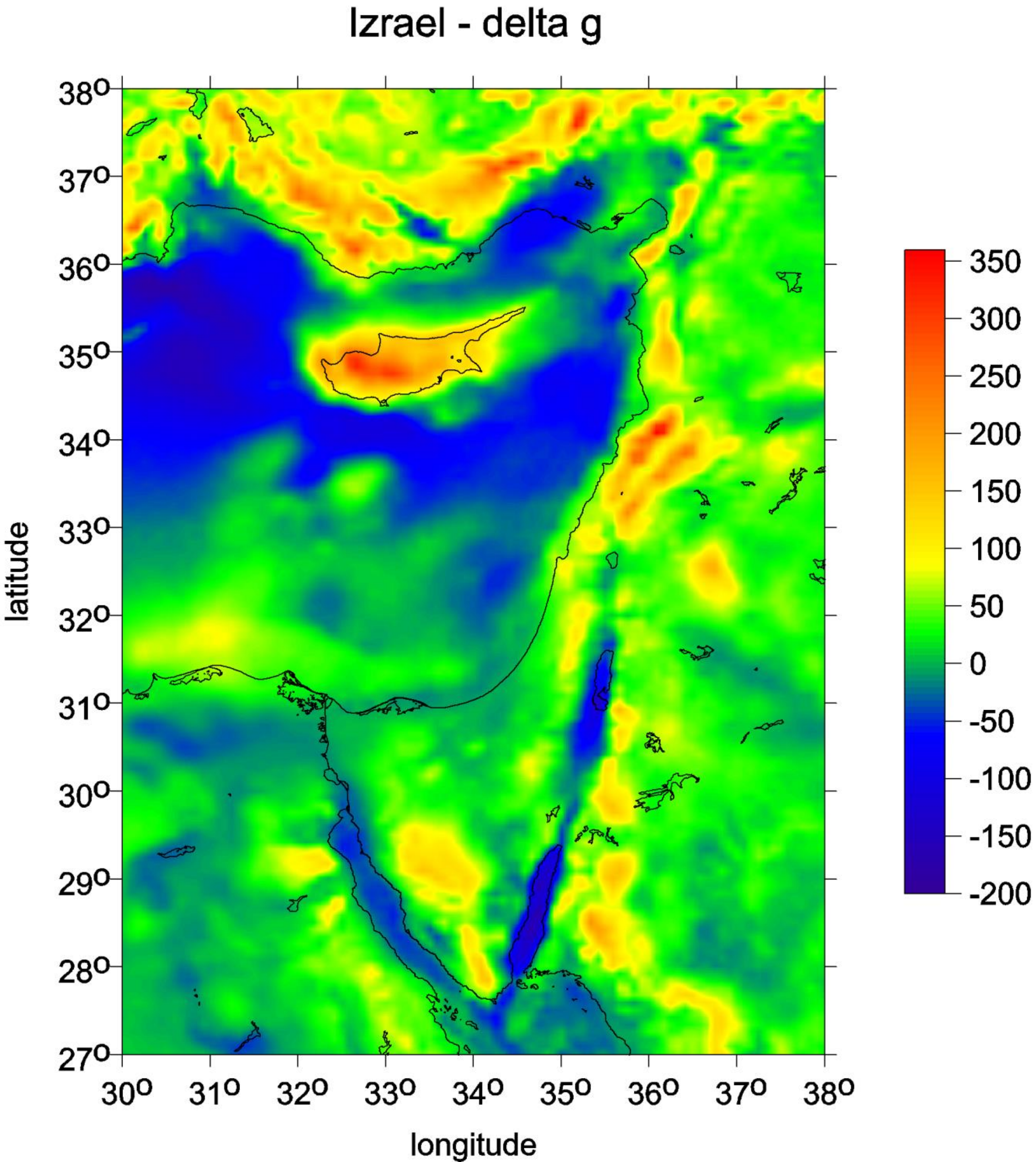

example Δg
[mGal]

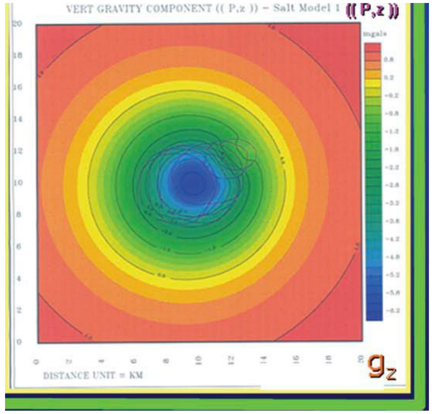

Δg

full

Marussi tensor

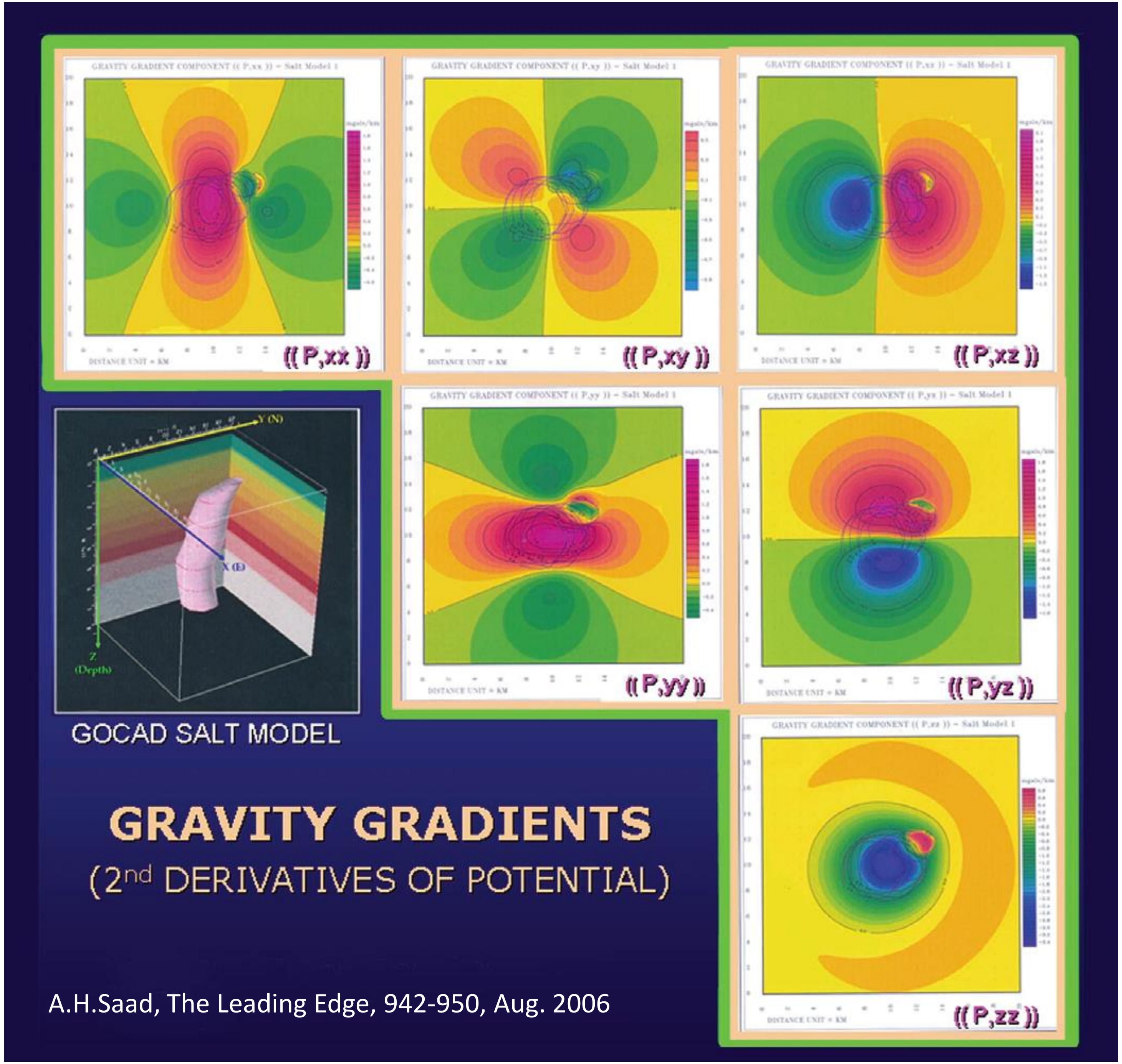

A.H.Saad, The Leading Edge, 942-950, Aug. 2006

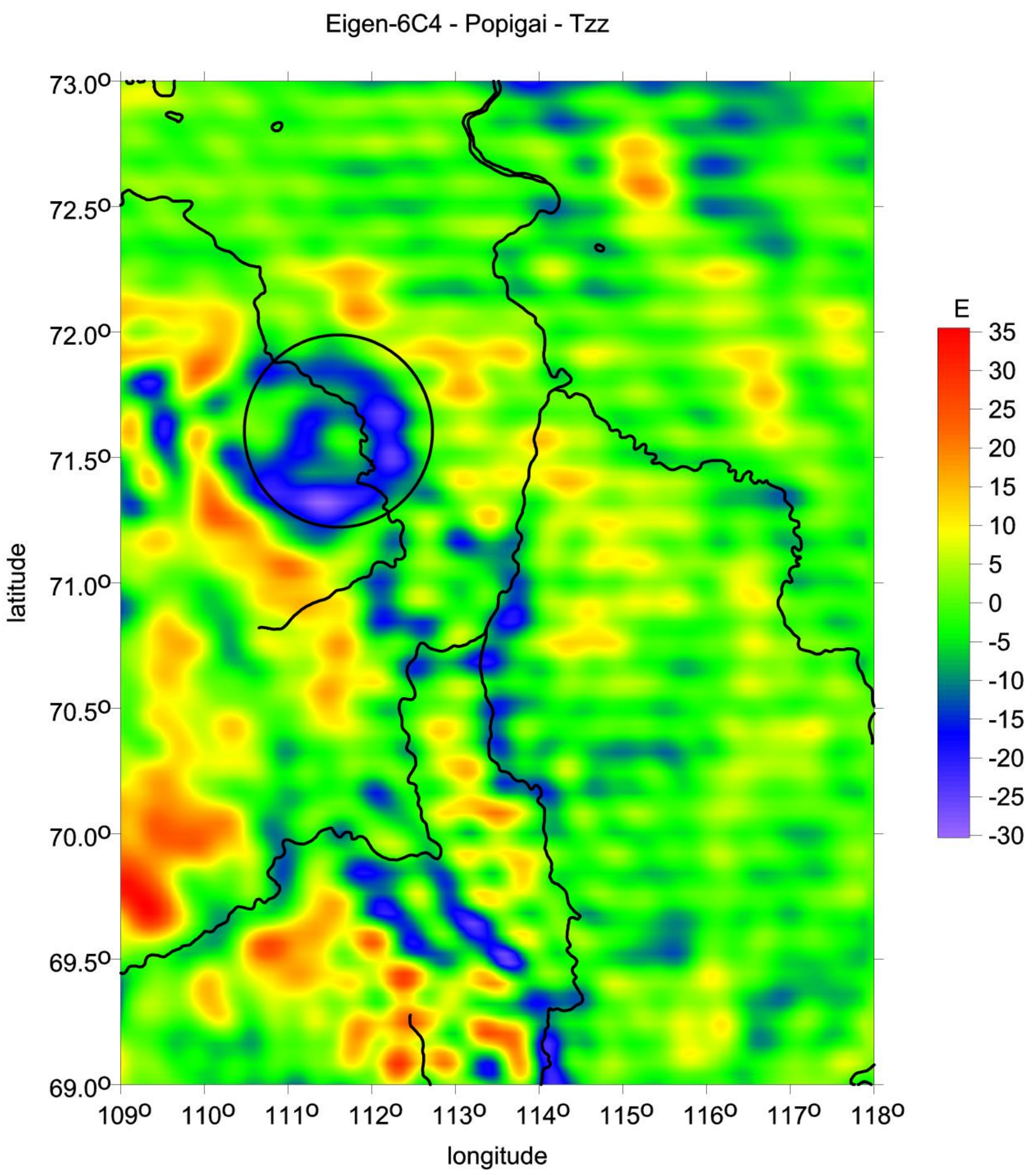
Eigen-6C4 - Popigai - Tzz
latitude
longitude
73.0°
72.5°
72.0°
71.5°
71.0°
70.5°
70.0°
69.5°
69.0°
109°
110°
111°
112°
113°
114°
115°
116°
117°
118°
E
35
30
25
20
15
10
5
0
-5
-10
-15
-20
-25
-30

Under any coordinate transformation, **Γ** preserves just 3 ***INVARIANTs***

$$I_0 = trace\ (\boldsymbol{\Gamma}) = T_{xx} + T_{yy} + T_{zz} = 0$$

$$I_1 = (T_{xx}T_{yy}+T_{yy}T_{zz}+T_{xx}T_{zz}) - (T_{xy}^2+T_{yz}^2+T_{xz}^2) = \frac{1}{2}\sum_{\{i,j\}\in\{x,y,z\}}\left(T_{ii}T_{jj} - T_{ij}^2\right)$$

$$I_2 = det\ (\boldsymbol{\Gamma}) = (T_{xx}(T_{yy}T_{zz}-T_{yz}^2) + T_{xy}(T_{yz}T_{xz} - T_{xy}T_{zz}) + T_{xz}\ (T_{xy}T_{yz}-T_{xz}T_{yy}).$$

Pedersen & Rasmussen (1990) showed that
the *ratio I of* $\boldsymbol{I_1}$ *and* $\boldsymbol{I_2}$ (dimensionless) defined as

$$0 \le I = -\frac{(I_2/2)^2}{(I_1/3)^3} \le 1$$

lies between 0 and 1 for any potential field. If the causative body is strictly 2D, then I = 0.

The *strike angle* ϑ_s (also known as strike lineaments or strike direction) is defined as

$$\tan 2\theta_s = 2\ \frac{T_{xy}\left(T_{xx}+T_{yy}\right)+T_{xz}T_{yz}}{T_{xx}^2-T_{yy}^2+T_{xz}^2-T_{yz}^2} = 2\,\frac{-T_{xy}T_{zz}+T_{xz}T_{yz}}{T_{xz}^2-T_{yz}^2+T_{zz}(T_{xx}-T_{yy})}$$

within a multiple of π/2. Mathematically the strike angle indicates the main direction of the Marussi tensor.
Geophysically it tells about the main direction of certain stresses.
Provided that the ratio I is small, the strike angle informs about a dominant 2D structure.
For more details see Beiki & Pedersen (2010) or Murphy & Dickinson (2009).

example invariant I_2 [s-6]

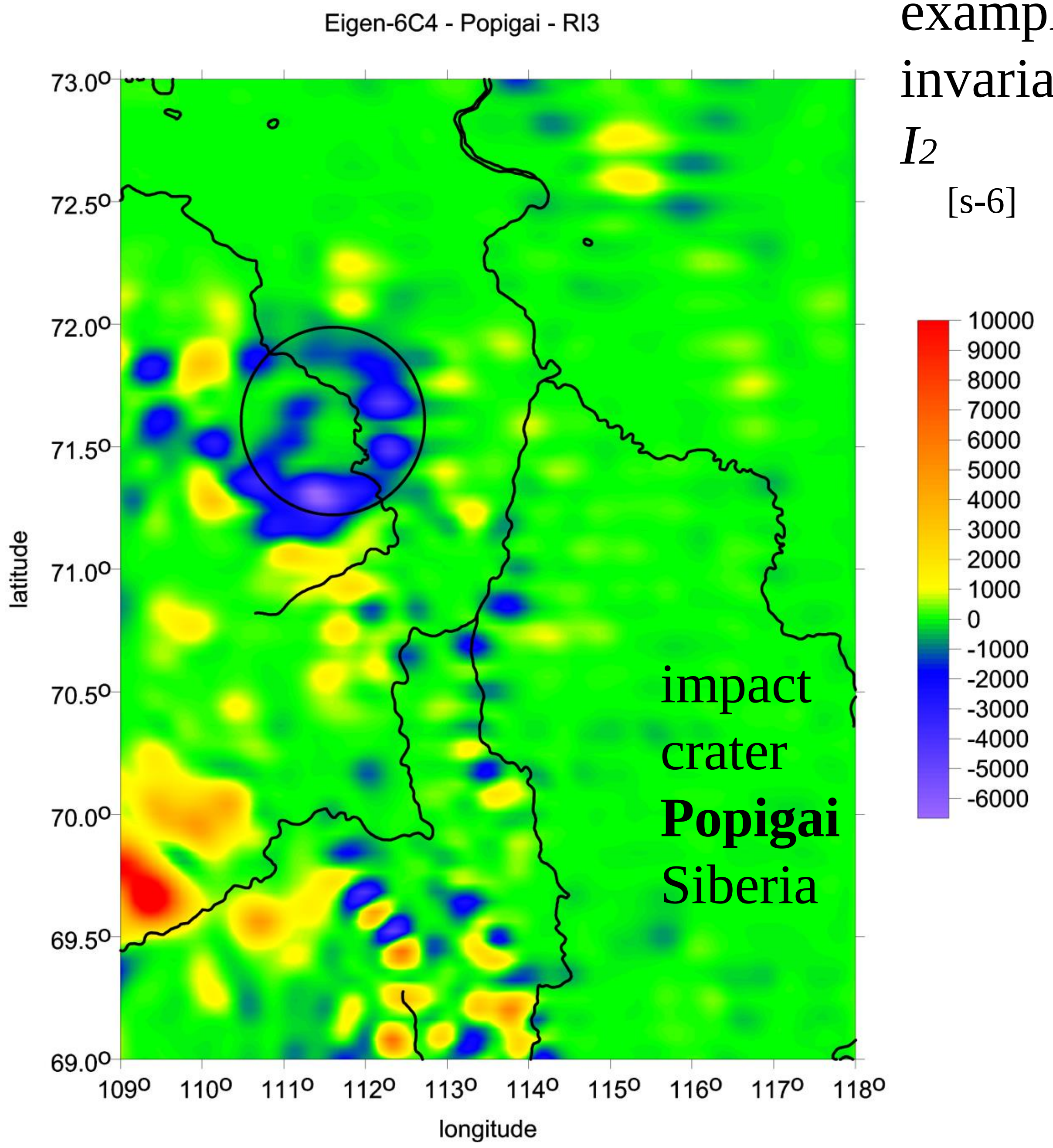

impact crater **Popigai** Siberia

example of strike angles θ [deg]

impact crater **Vredefort**, South Africa
halo from the combed strike angles

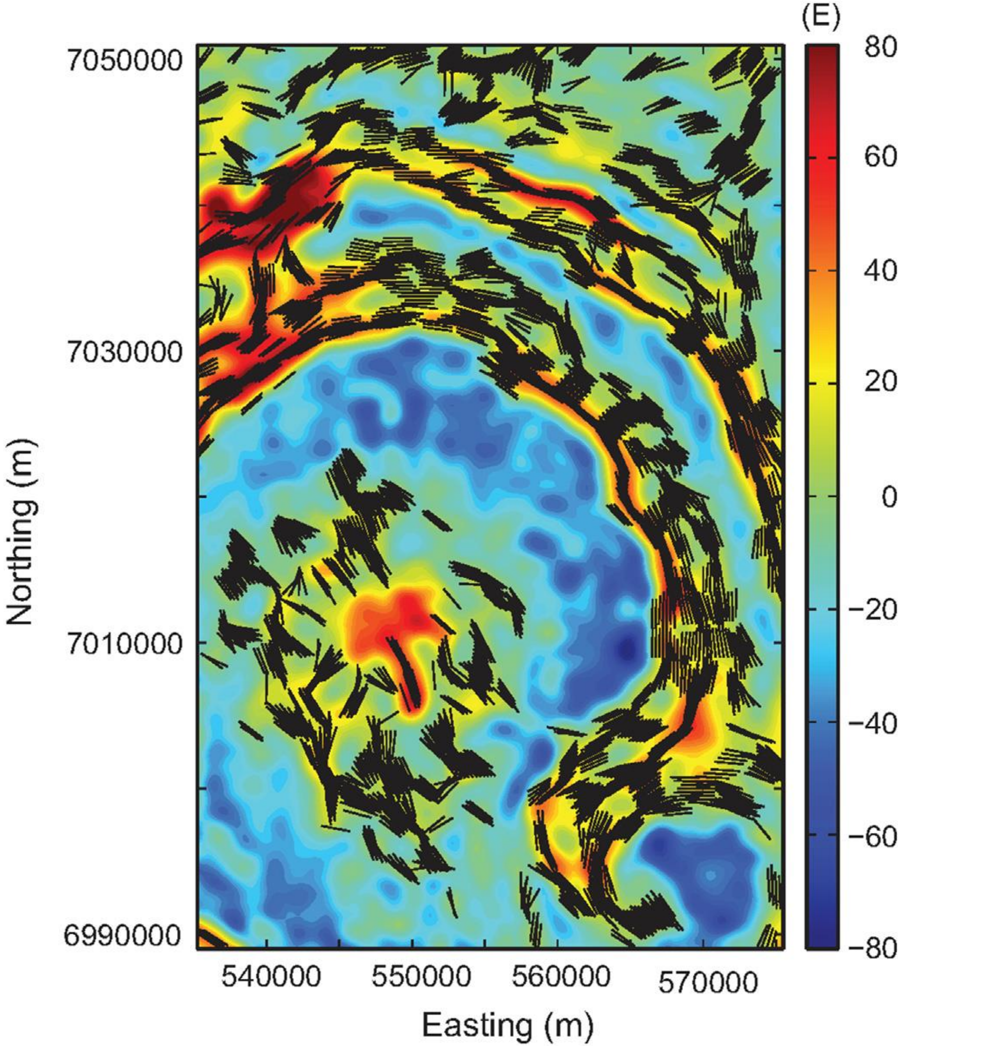

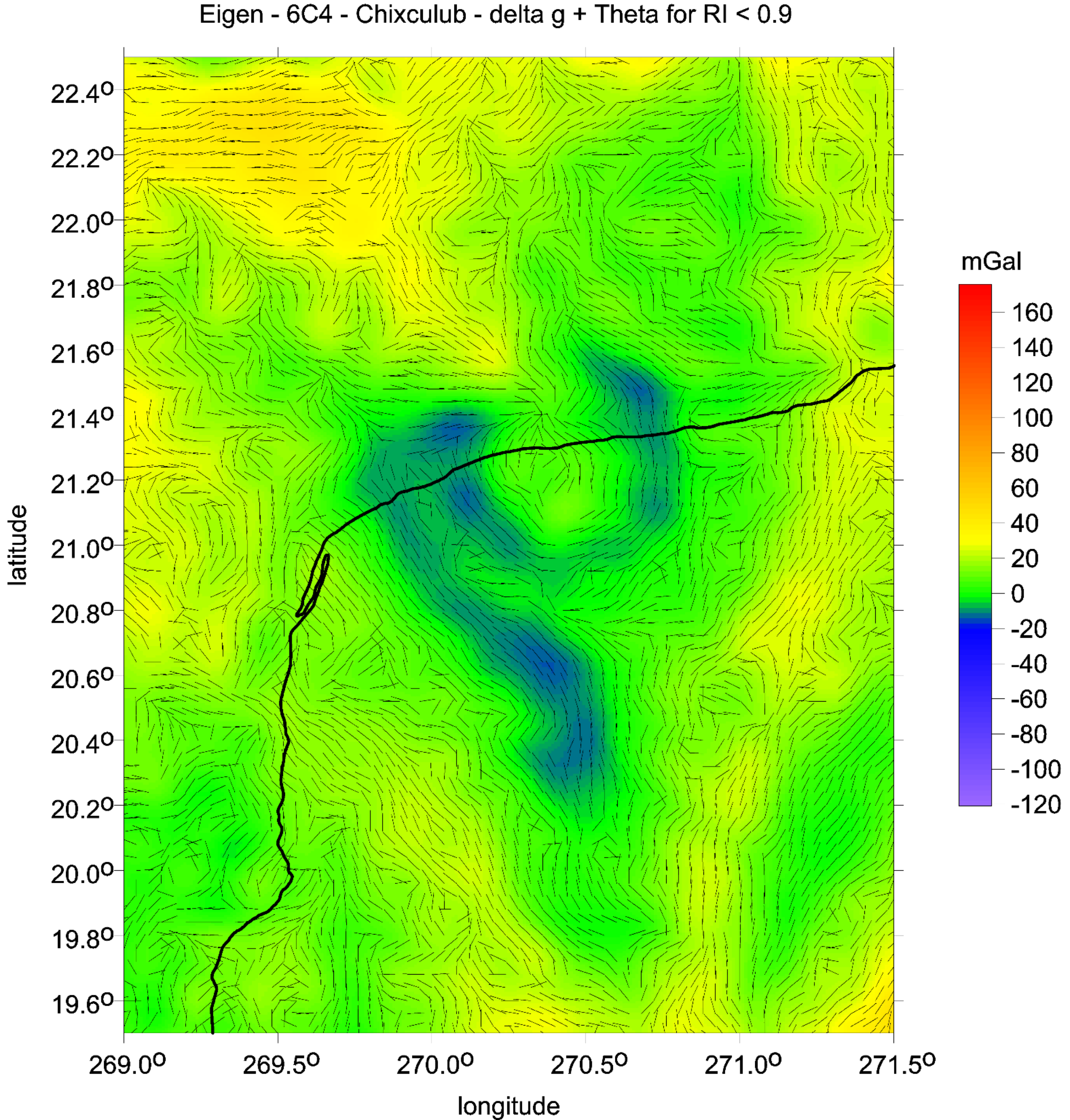

example

Δg and θ

[mGal], [deg]

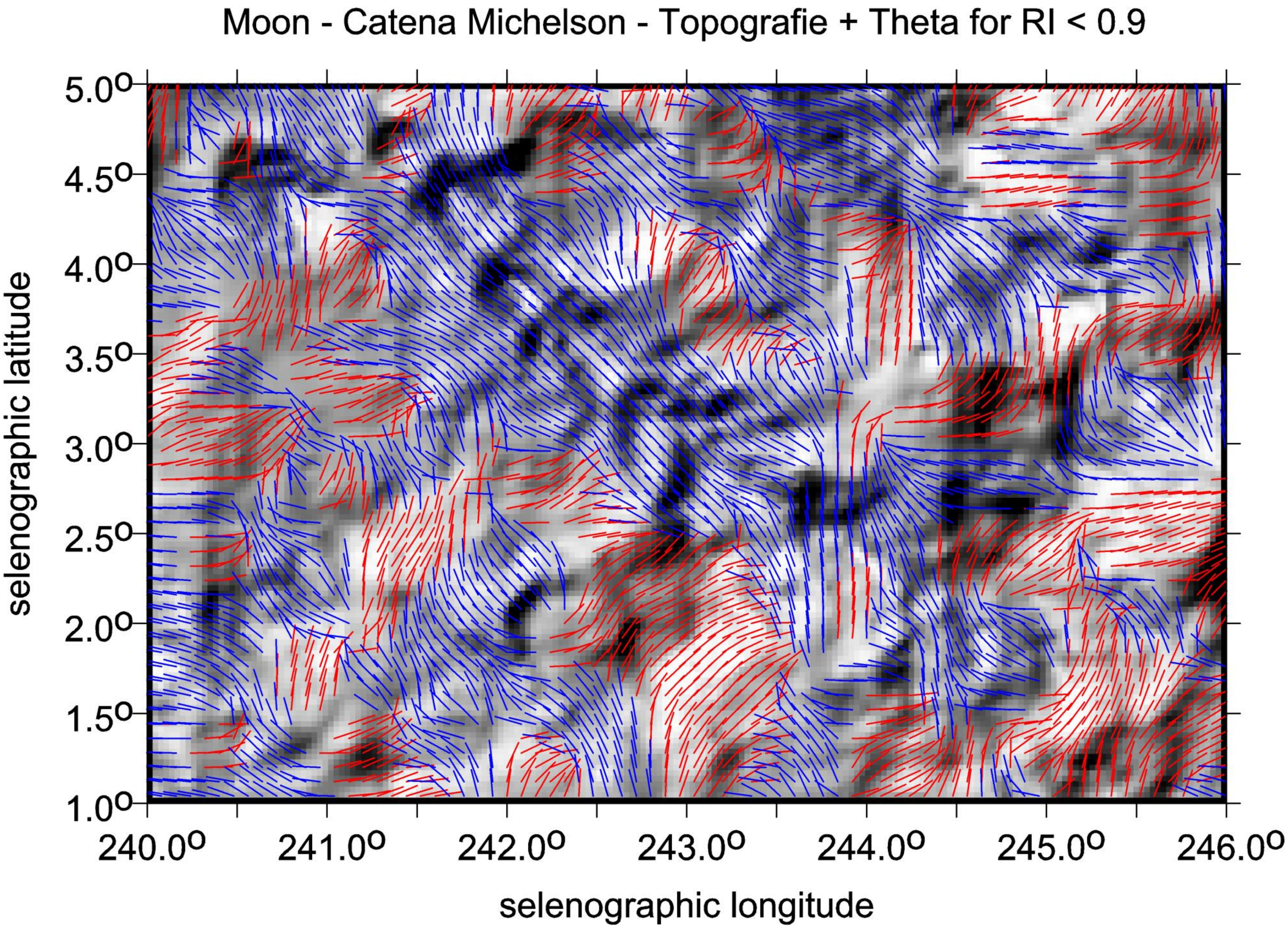

The Moon

example of θ

[deg]

plus topography

Virtual deformations (Kalvoda *et al.* 2012, Klokočník *et al.* 2013)

directions of such a deformation due to "erosion" brought about solely by "gravity origin".
If there would be a tidal potential *T*, then the horizontal shifts (deformations) would exist due to it and they could be expressed

in north-south direction (latitude direction) … [left] and in east-west direction (longitudinal direction) … [right]

$$u_\Phi = l_S \frac{1}{g} \frac{\partial T}{\partial \varphi} \qquad u_\Lambda = l_S \frac{1}{g \cos \varphi} \frac{\partial T}{\partial \lambda}$$

where *g* is the gravity acceleration 9.81 $m \cdot s^{-2}$,
l_S is the elastic coefficient (Shida number) expressing the elastic properties of the Earth as a planet (l_S = 0.08),
φ and λ are the geocentric coordinates (latitude and longitude) of a point *P* where we measure *T*
The apparatus of mechanics of continuum to derive the main directions of the tension is applied (see, e.g., Brdička *et al.* 2000).
The tensor of (small) deformation ***E*** is defined as a gradient of shift. It holds that

$$\boldsymbol{E} = \begin{pmatrix} \epsilon_{11} & \epsilon_{12} \\ \epsilon_{21} & \epsilon_{22} \end{pmatrix} = \begin{pmatrix} \frac{\partial u_x}{\partial x} & \frac{\partial u_x}{\partial y} \\ \frac{\partial u_y}{\partial x} & \frac{\partial u_y}{\partial y} \end{pmatrix}$$

The tensor ***E*** can be separated into two parts:

$$\boldsymbol{E} = \mathbf{e} + \boldsymbol{\Omega} = (\mathrm{e_{ij}}) + (\Omega_{\mathrm{ij}})$$

where **e** is the symmetrical tensor and ***Ω*** the anti-symmetrical tensor of deformation, respectively. The symmetrical tensor is

$$\mathbf{e} = \begin{pmatrix} \mathrm{e}_{11} & \mathrm{e}_{12} \\ \mathrm{e}_{21} & \mathrm{e}_{22} \end{pmatrix} = \begin{pmatrix} \epsilon_{11} & (\epsilon_{12}+\epsilon_{21})/2 \\ (\epsilon_{12}+\epsilon_{21})/2 & \epsilon_{22} \end{pmatrix}$$

and the parameters of deformation are:

$\Delta = e_{11} + e_{22}$	total dilatation	$\boldsymbol{a} = \frac{1}{2}(\Delta + \gamma)$	**major semi-axis of ellipse of deformation**
$\gamma_1 = e_{11} - e_{22}$	pure cut	$\boldsymbol{b} = \frac{1}{2}(\Delta - \gamma)$	**minor semi-axis of ellipse of deformation**
$\gamma_2 = 2e_{12}$	technical cut	$\alpha = \frac{1}{2} \operatorname{atan}(\gamma_2 / \gamma_1)$	direction of main axis of deformation
$\gamma = (\gamma_1^2 + \gamma_2^2)^{1/2}$	total cut		

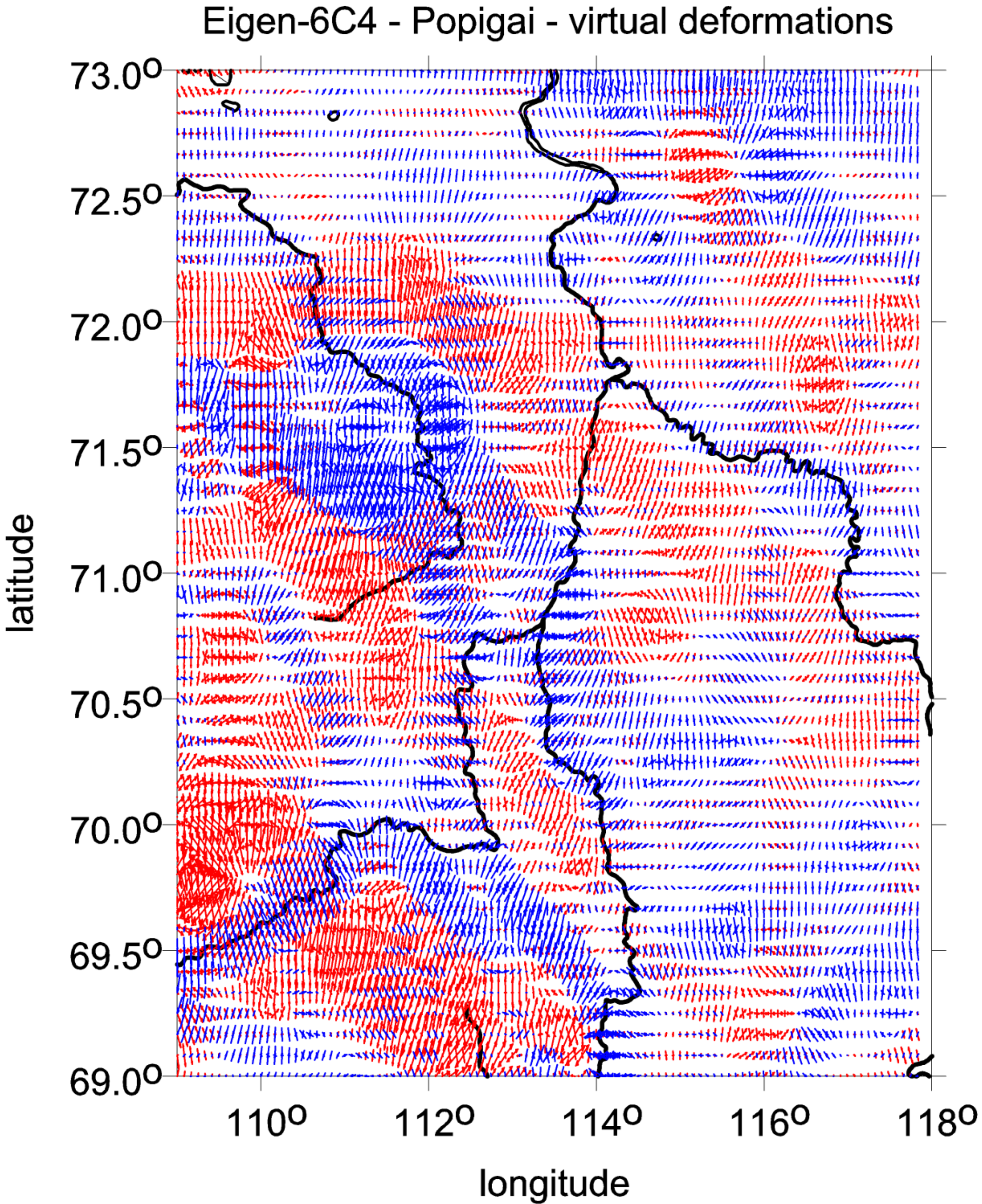

Eigen-6C4 - Popigai - virtual deformations
73.0°
72.5°
72.0°
71.5°
71.0°
70.5°
70.0°
69.5°
69.0°
latitude
110°
112°
114°
116°
118°
longitude

Mare Orientale

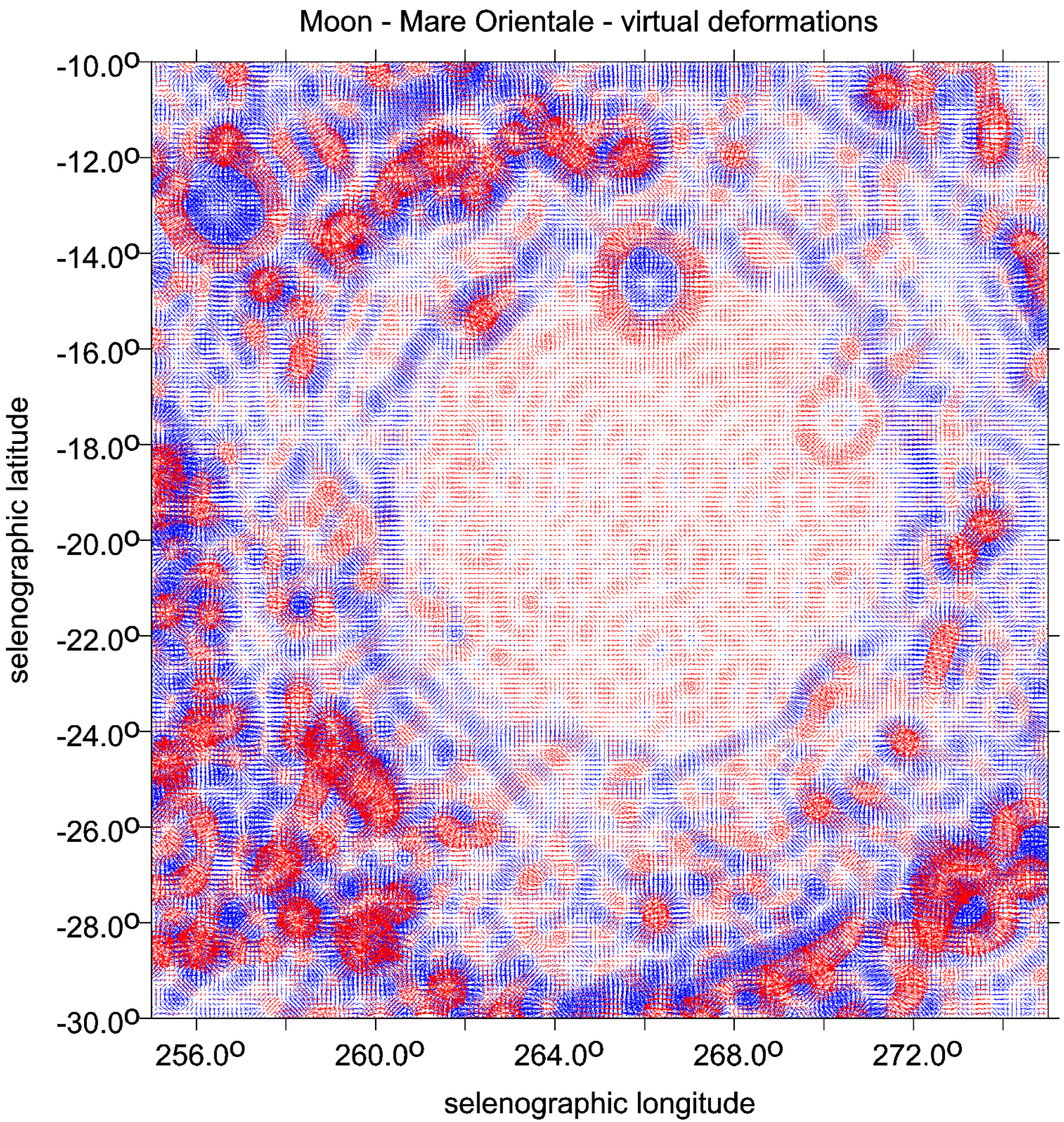

virtual deformations

example *vd*

[-]

dilatation in red
compression in blue

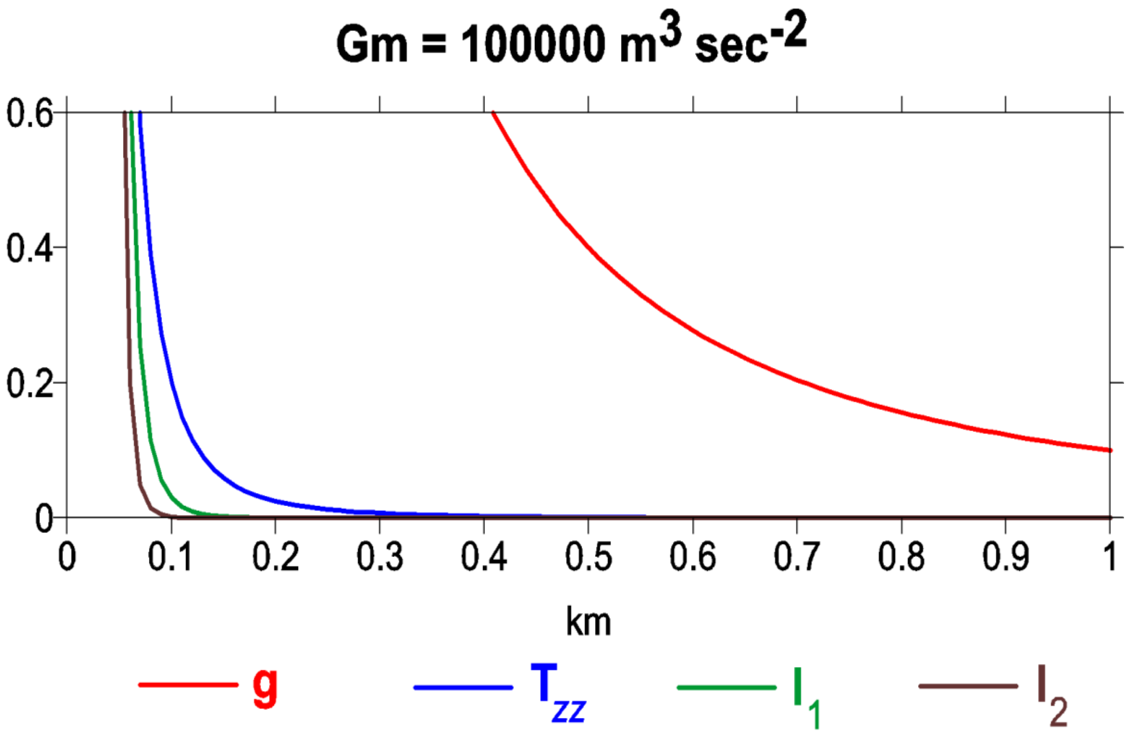

An example of decrease of the values of the gravity aspects of a spherical model of gravitational potential with increasing distance (depth) from their source (density anomaly, causative body).

On the *x* axis,there are depths in kilometres, on the *y* axis, there is an arbitrary quantity (for a simple intercomparison). This is an illustrative case for a **mass point** with randomly selected value of *GM* (here *Gm*, representing a spherical ground density anomaly).

The strike angles among other gravity aspects

The *strike angles* θ [deg]

(strike directions) are defined as follows (Pedersen and Rasmussen 1990):

$$\tan 2\theta = 2\,\frac{T_{xy}(T_{xx}+T_{yy})+T_{xz}T_{yz}}{T_{xx}^2-T_{yy}^2+T_{xz}^2-T_{yz}^2} = 2\,\frac{-T_{xy}T_{zz}+T_{xz}T_{yz}}{T_{xz}^2-T_{yz}^2+T_{zz}(T_{xx}-T_{yy})}$$

ambiguous within a multiple of π/2;

where T_{ij} are the components of the *Marussi tensor* **Γ** (i.e. the *tensor of the gravity gradients or second derivatives of the disturbing potential*.

These are non-linear combinations of the harmonic geopotential coefficients.

The combed strike angle

Strike angles aligned. Being combed, the strike angle indicates existence of impact craters, or task deposits, but yields no proof of them; the indication is not unambiguous as for oil&gas, it may indicate water, ground water, wadi, deep valley, trench, may be also coal; further information needed (topography, geology,…) for specific decision…

combed strike angles in the studied area,
one way oriented strike angles

comb factor → 1

disheveled strike angles in the studied area =
= strike angles are in diverse directions

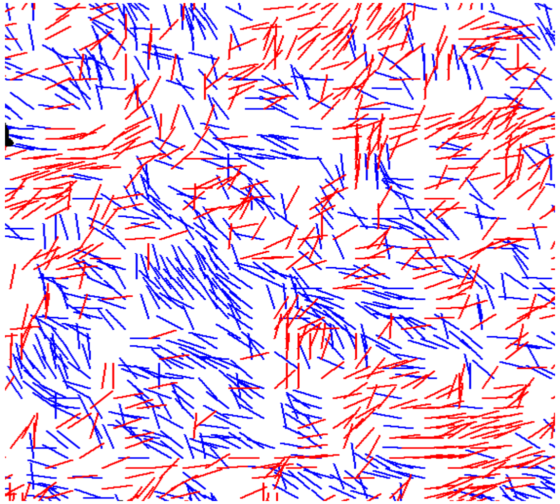

comb_factor → 0

For statistical use we defined the comb coefficient *Comb* as a relative value in the interval ⟨0,1⟩, where 0 means „not combed“ (totally disheveled, the vectors θ are in diverse directions) and *1* „combed“ (perfectly kempt, the vectors of θ are oriented into one prevailing direction). If *Comb* is smaller than 0.55, we say that θi of the given region are „not combed“; if *Comb*>0.65, we say θi are „combed“.

The *combed strike angles* are oriented roughly in one direction, linearly or around a circular structure.

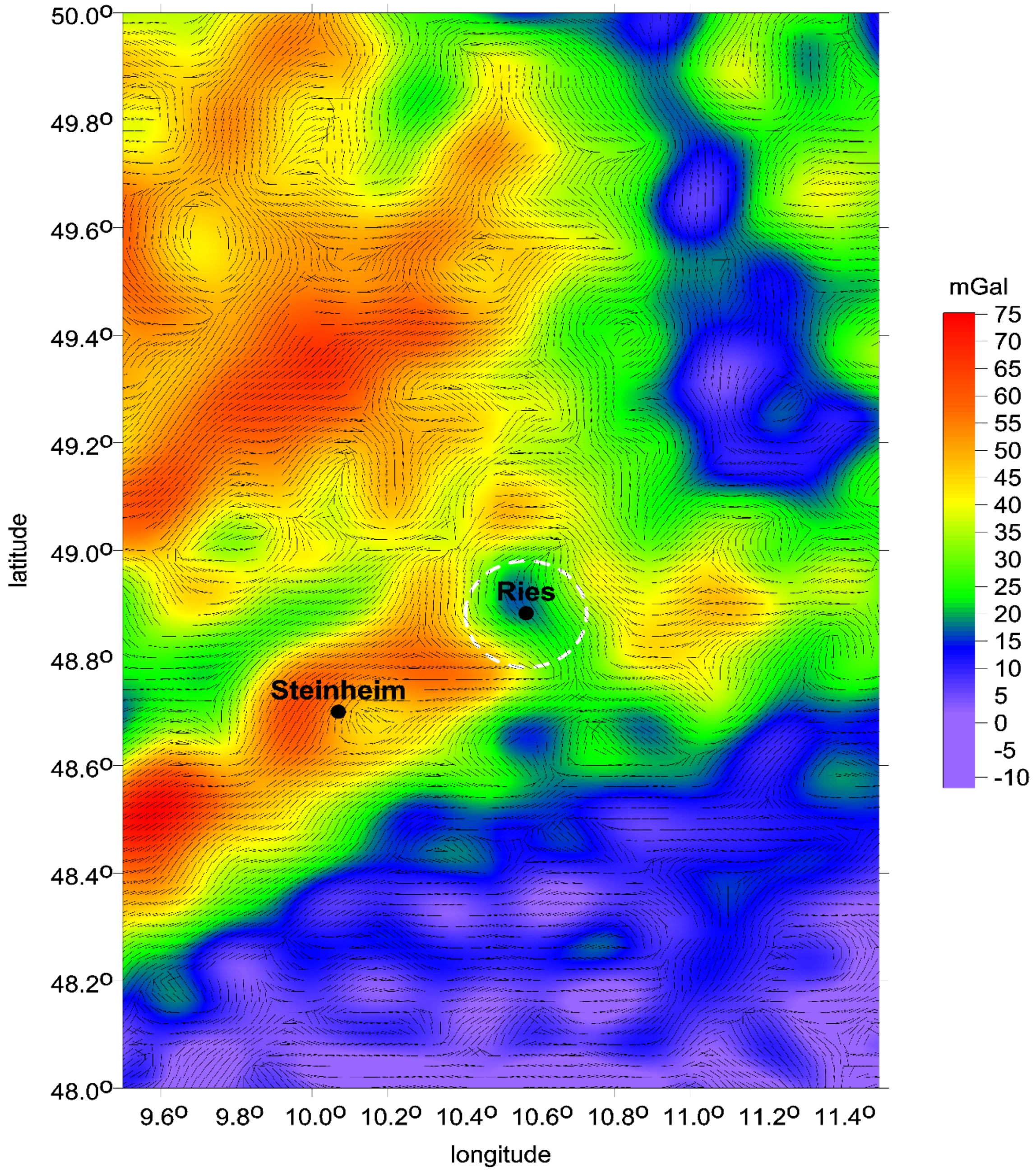

Steinheim and Ries impact craters (Germany) as depicted by the combed strike angles with the gravity anomalies EIGEN 6C4

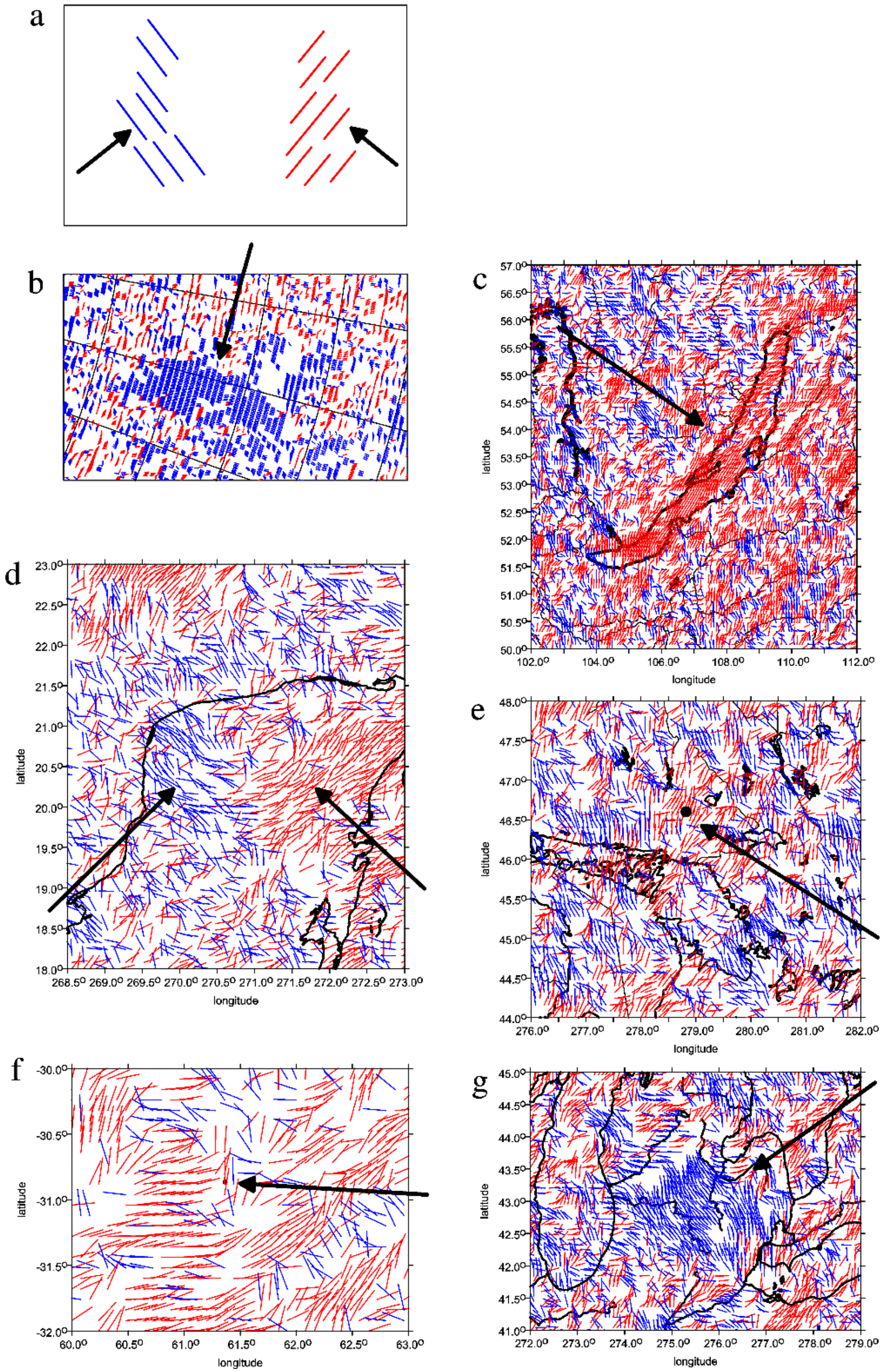

Strike angles for the impact angle – tutorial

a theory
b Lake Vostok, Antarctica
c Lake Bajkal, Russia
d impact crater Chicxulub, north Yucatan
e impact crater Sudbury, Canada
f probable impact crater Burckle, Indian Ocean
g Saginaw Bay, the Great Lakes, USA

The arrows show direction rectangular to the direction of the strike angles
red colour means their direction to the west and blue to the east of the local meridian

RET-2014-Vostok-Theta-

sever vpravo

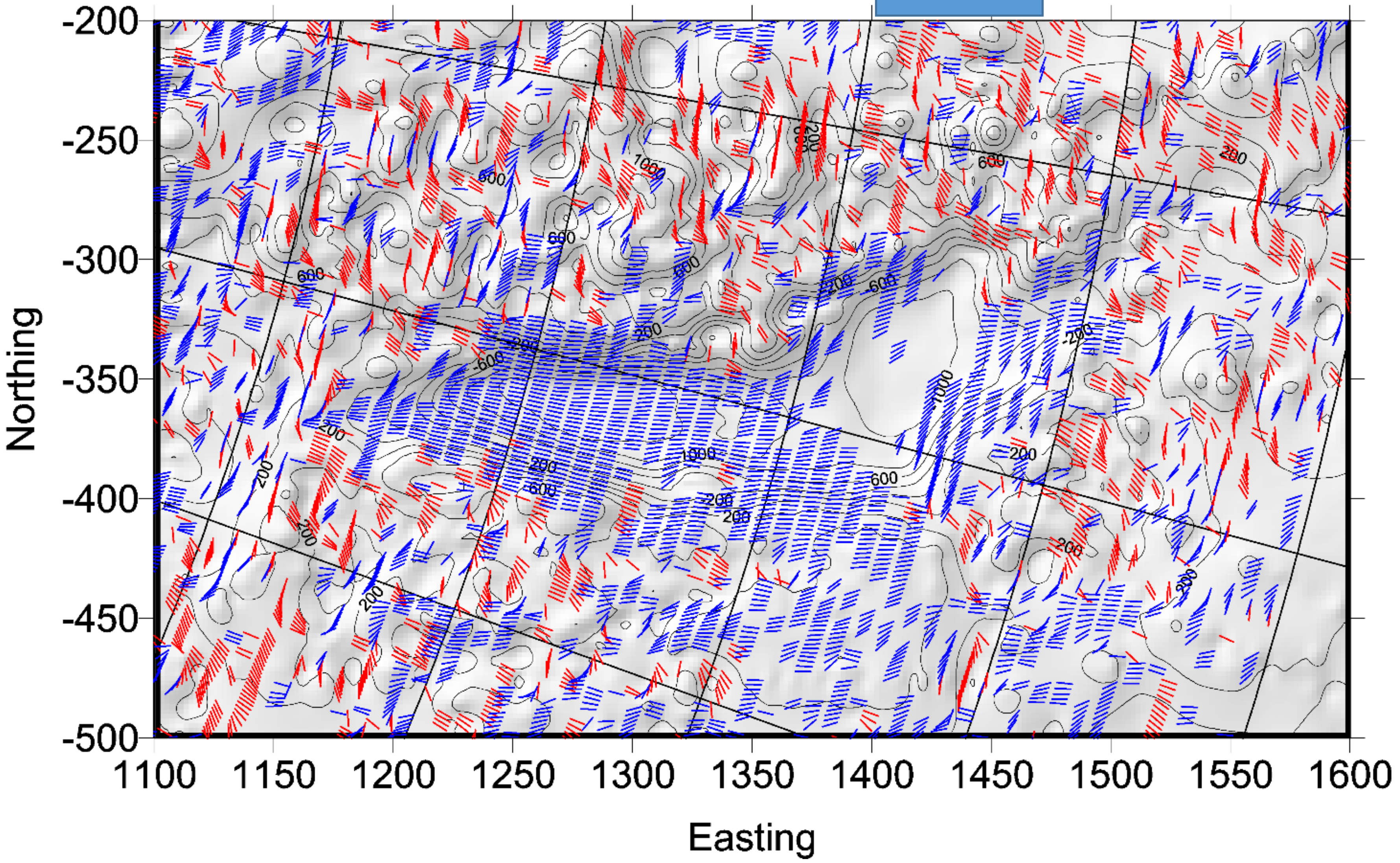

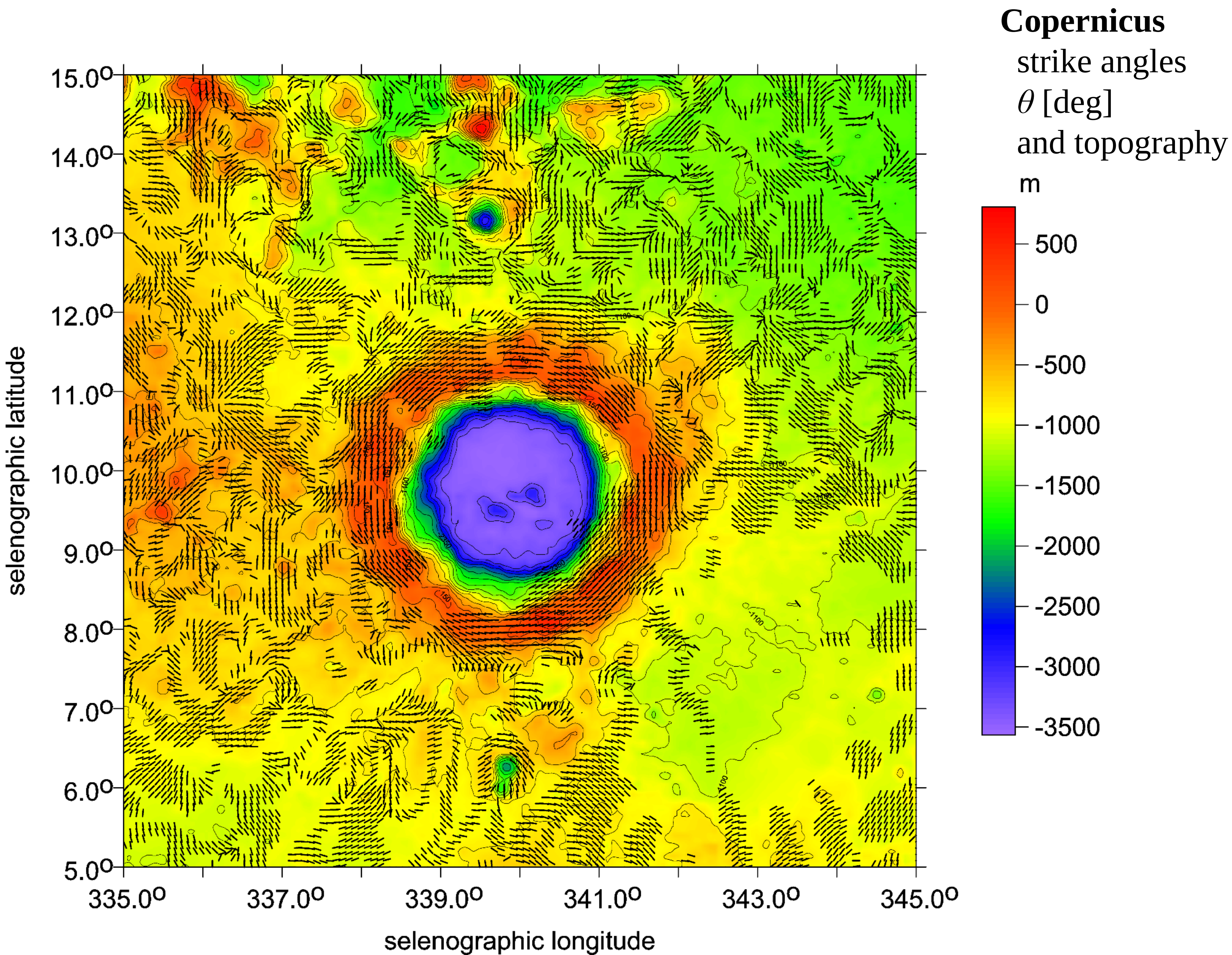
Copernicus
strike angles
θ [deg]
and topography
m
500
0
-500
-1000
-1500
-2000
-2500
-3000
-3500
15.0°
14.0°
13.0°
12.0°
11.0°
10.0°
9.0°
8.0°
7.0°
6.0°
5.0°
selenographic latitude
335.0°
337.0°
339.0°
341.0°
343.0°
345.0°
selenographic longitude

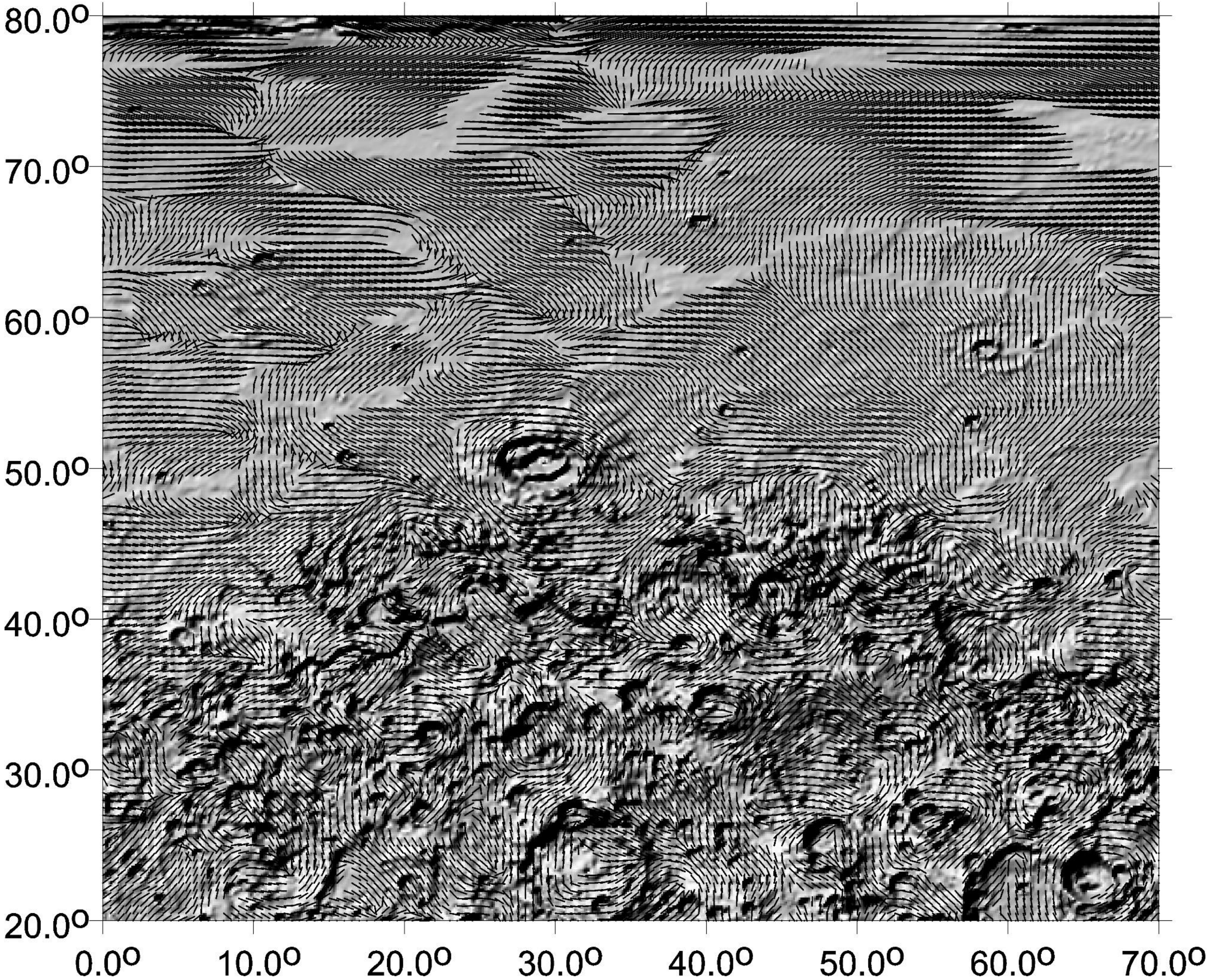
80.0°
70.0°
60.0°
50.0°
40.0°
30.0°
20.0°
0.0°
10.0°
20.0°
30.0°
40.0°
50.0°
60.0°
70.0°

Ground Resolution

A usual simple estimate of the smallest representable feature of the gravity field or the **shortest half-wavelength L_{half} (as a distance on a sphere) that can be resolved with all C_{lm}, S_{lm} to L_{max}, is**

$$L_{half} = \pi R / L_{max}$$

or equivalently, taking the circumference $2\pi R$ = 40 050 km for the Earth:

$$L_{half} = 2 \pi R / (2 L_{max}) = 40\,050 / (2 L_{max}).$$

This L_{half} is what we call the "ground resolution". For L_{max}= *300* and *2190,* we have L_{half} = 67 and 9 km, respectively. The former limit roughly corresponds to the resolution of the GOCE data alone, and the latter belongs to the combined models, EGM 2008, EIGEN 6C4 or SatGavRET2014 (in the case of the Earth).

Body	R [km] rounded	max *d/o* of model used	resolution [km]
Earth	6380	2190	9
Moon	1740	600	9
Mars	3400	80-120	130-90
Venus	6050	120	160

Artefacts - theoretical notes   Truncation error tests   Danger of misinterpretations

We quote from Klokočník et al. (2021), where we distinguished various types of artefacts:

(i) G*raining* of the signal when increasing the resolution of the computed parameter from the data set of not sufficient quality. The graining is increasing with increasing demands leading to a total disintegration, break-up, dispersion of the signal. The graining can be understood as an indicator of a forthcoming failure in the "high resolution" result. The artefact is defined by graining and that a failure of a presenting the calculations. For example, there is a spherical harmonic expansion of quantity V to certain maximum degree and order (d/o), but beyond certain d/o the calculation solutions start diverging and the artefacts will appear.

(ii) Phantoming - odd, bizarre, fantastic, looking, for example, like long walls of various forms, pyramids, circles and other ghosts, partly due to lack of data, partly from processing procedures and software.

(iii) Data gapping (for example, regions with missing bedrock topography, regions with data from ice penetrating radars in Antarctica) may yield false smoothed signal, expressing featureless areas.

(iv) Aliasing appears when we attempt reconstructing the original waveform from its samples and we have not sufficient amount of such samples. Aliasing represents a long-wave artefact due to not sufficient sampling in frequency space (insufficient data density); the shorter frequencies can have real context but hidden due to aliasing. Aliasing produces features like barriers, bulwarks, mounds, valleys, lakes, pyramid-like objects.

(v) Striping, organized along-track of satellite orbit bearing the instrument providing the data. They originate due to the irregular satellite altitude, different instrument condition (night vs. day radiation exposure conditions, solar wind activity) data coverage and gaps. When we compare density of the data along-track to that cross-track orbital components, we see remarkable differences between these two: one is high, one is low. In the case of specialised, nearly polar geodetic satellites used for gravity field studies, the along-track component is roughly in SN/NS direction while the cross-track goes along longitudes WE/EW.

Low resolution

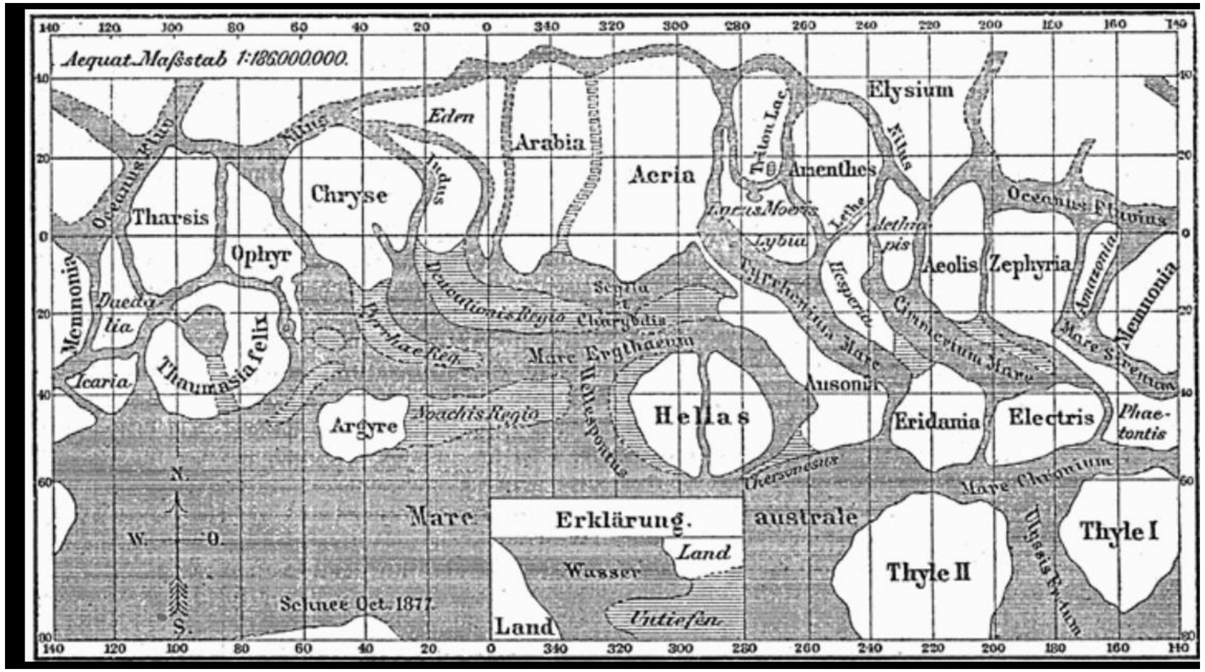

Historical map of planet mars from Giovanni Schiaparelli

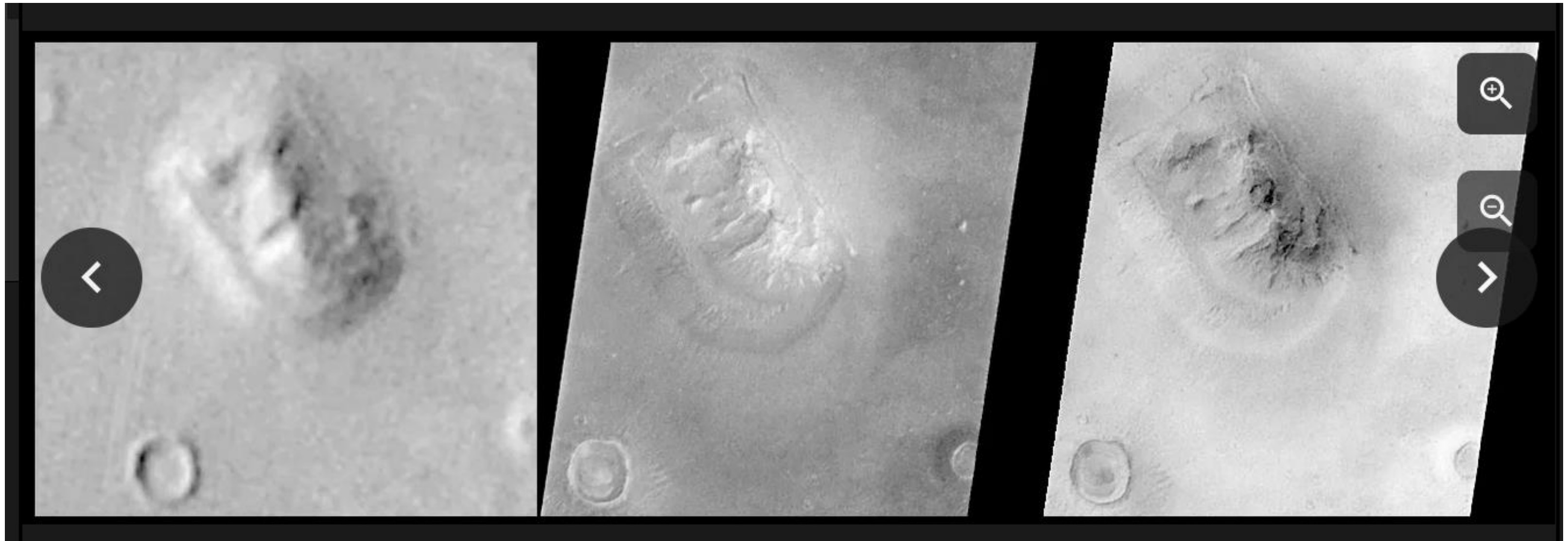

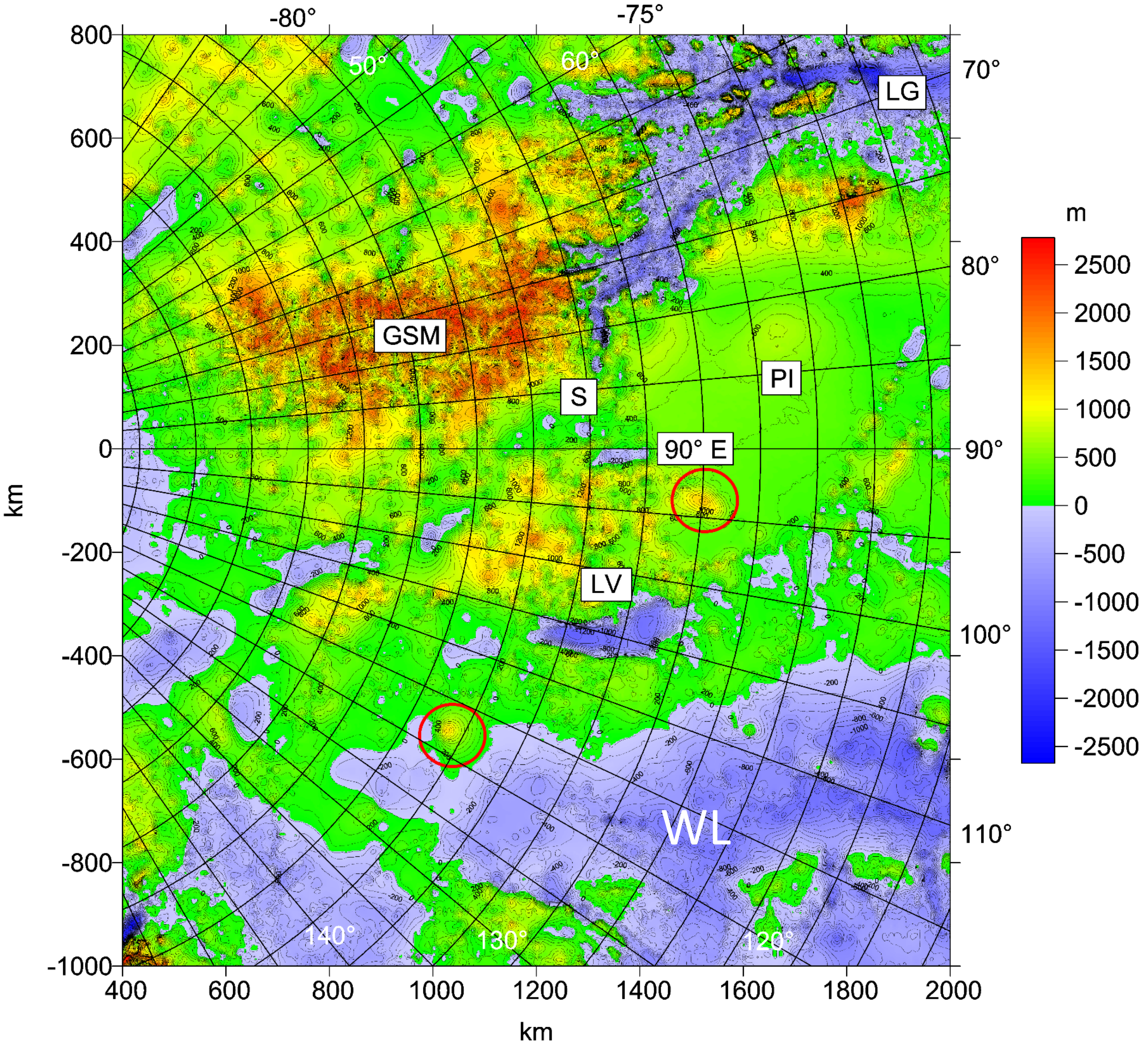

-80°
-75°
50°
60°
70°
80°
90°
100°
110°
140°
130°
120°
LG
GSM
S
PI
90° E
LV
WL
m
2500
2000
1500
1000
500
0
-500
-1000
-1500
-2000
-2500
km
800
600
400
200
0
-200
-400
-600
-800
-1000
400
600
800
1000
1200
1400
1600
1800
2000

we ask too much
than the data
may provide

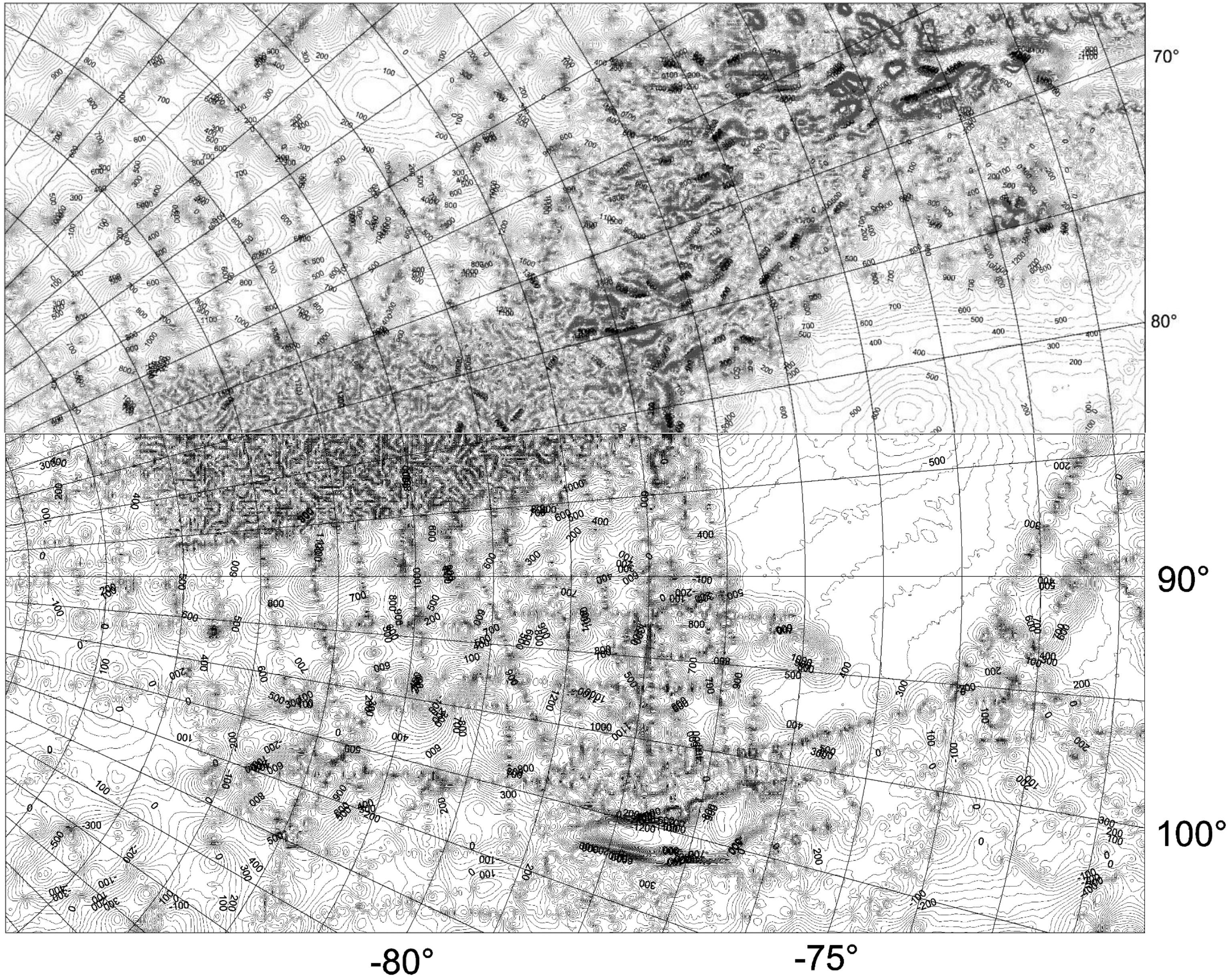

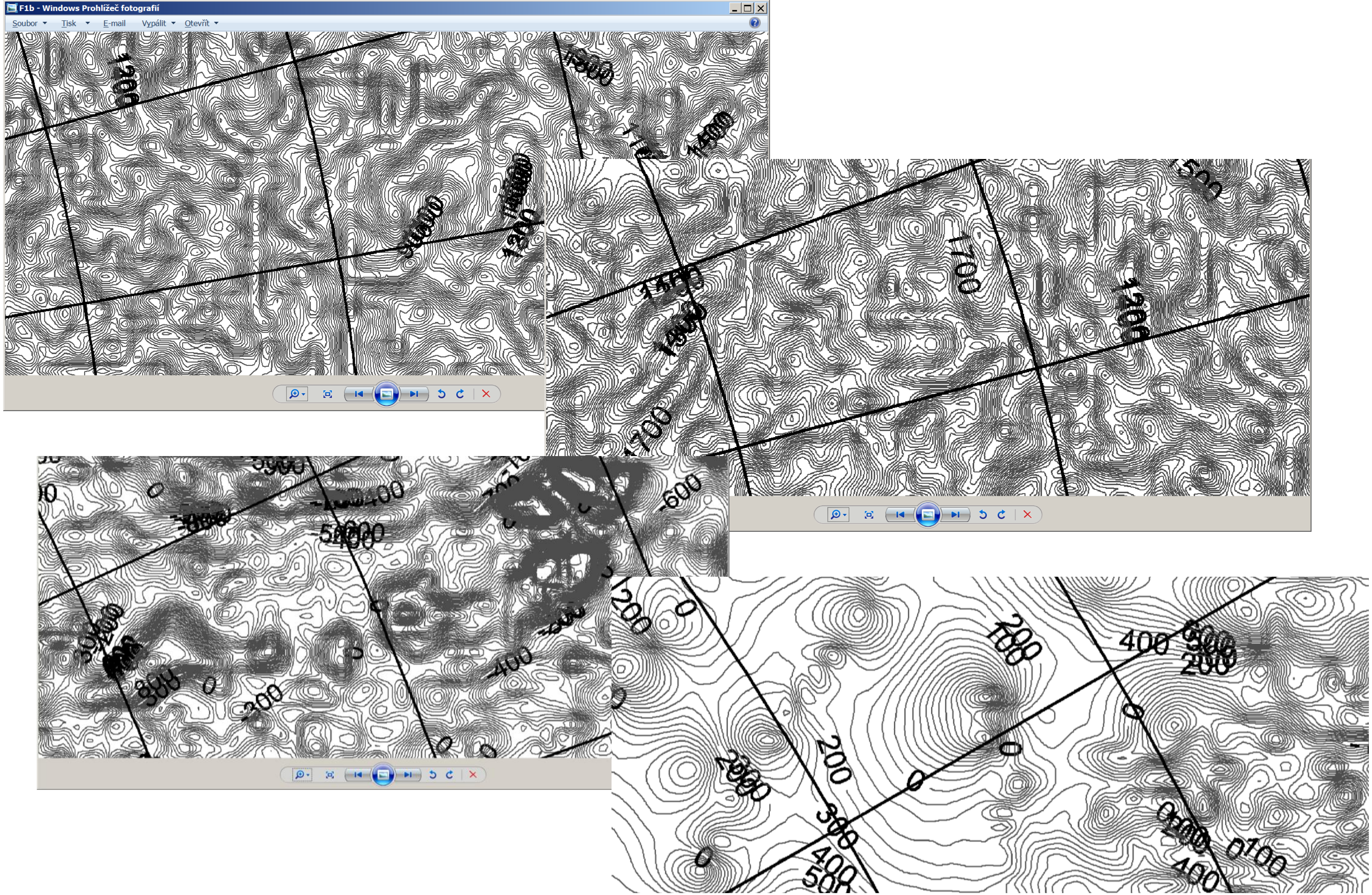
F1b - Windows Prohlížeč fotografií
Soubor
Tisk
E-mail
Vypálit
Otevřít
1200
1700
1700
1200
-600
-400
-200
200
200
200
400
300
400

respect maximum degree and order d/o of harmonic expansion in the given gravity field model recommended for practical use (by the authors of the model and based on truncation error tests)

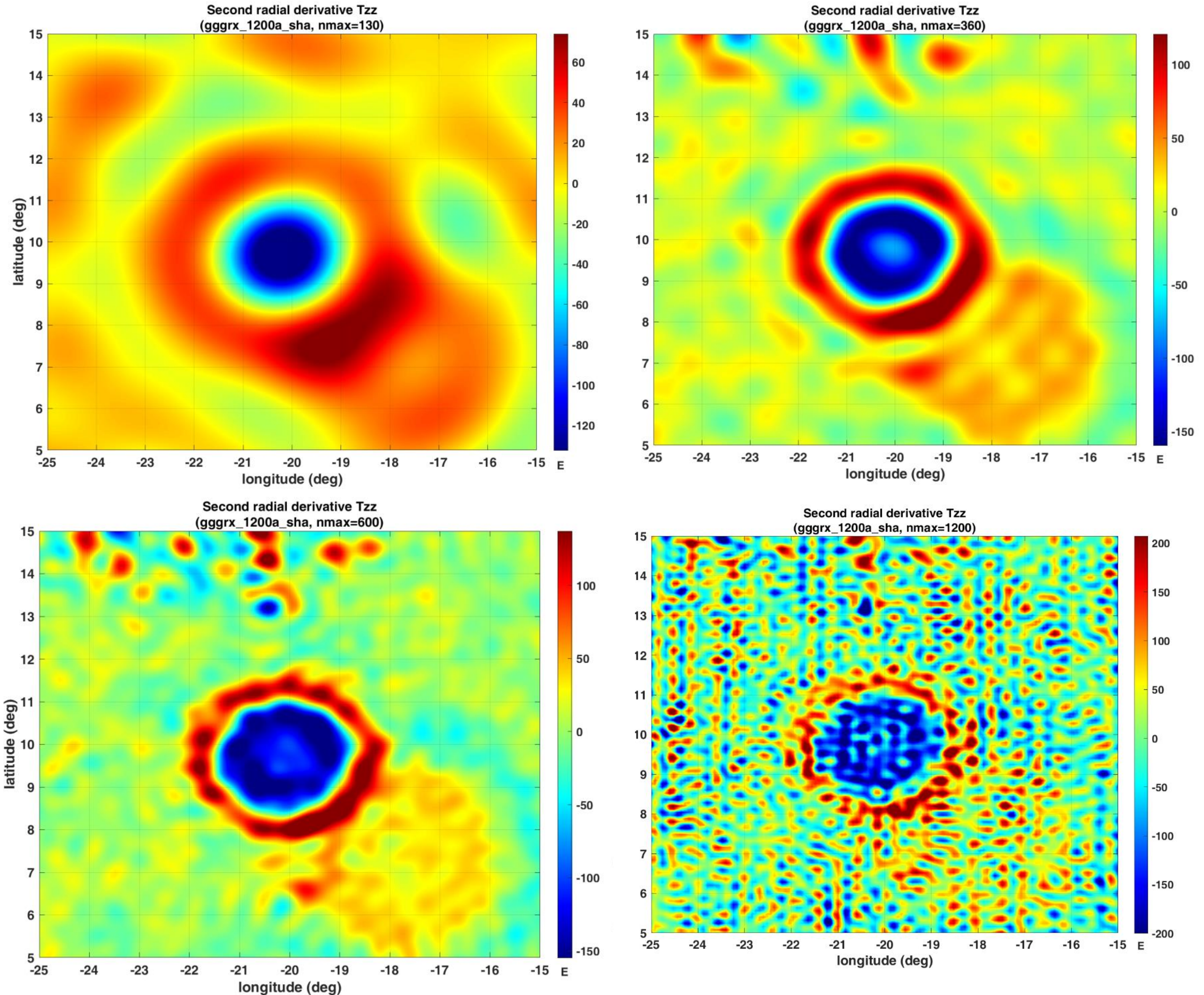

d/o

130 360

600 1200

Truncation error test for the Moon
with gravity anomalies

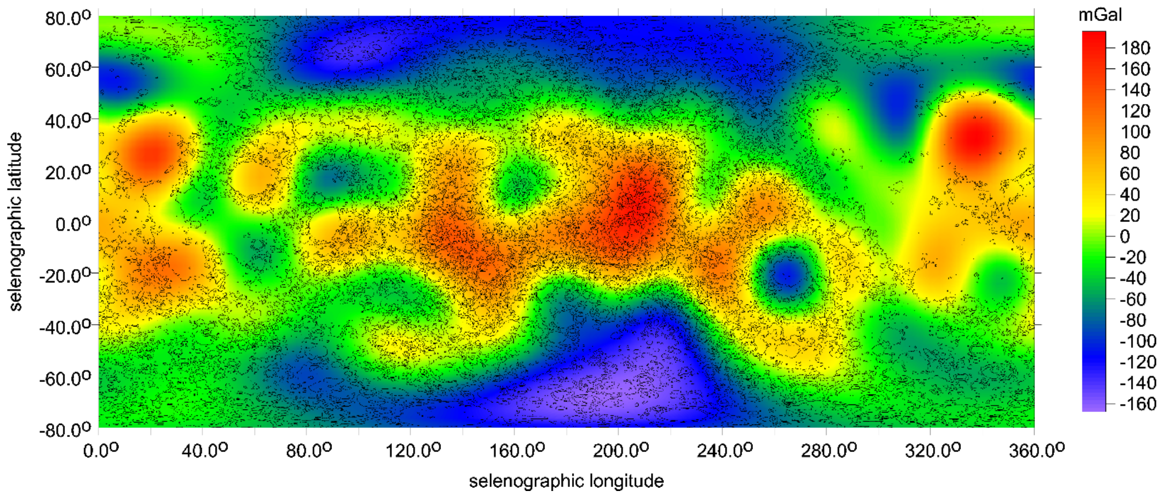

The main characteristics of the gravity field of the Moon, in terms of Δg [mGal], with the GRGM1200A model, but only to maximum d/o=10. The higher terms are cut. Compare to Fig. 81.2 or Fig. 3.3.2. The near side of the Moon has longitudes 0-90^0 and 270-360^0 E. LOLA topography [m] included.

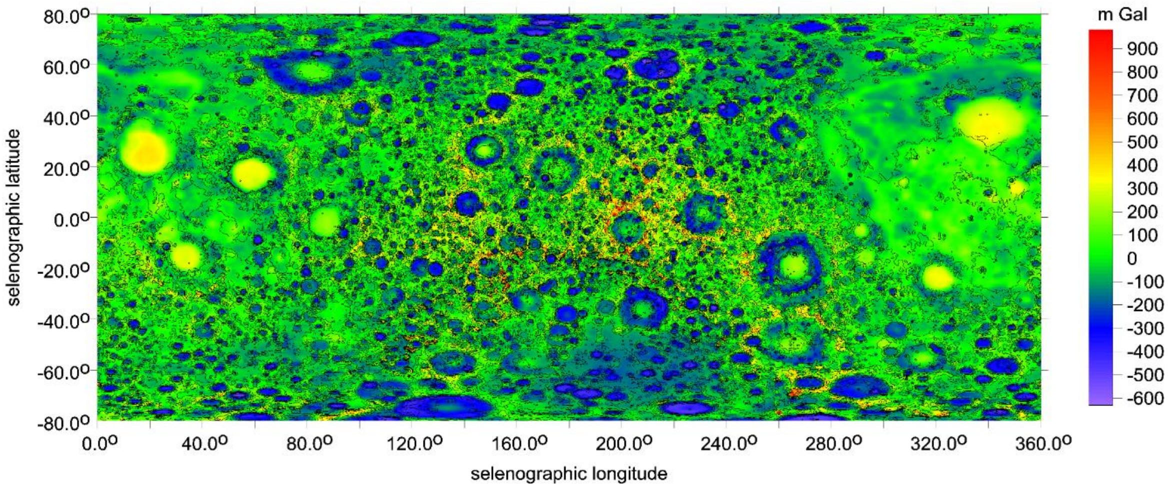

The gravity field of the Moon; Δg [mGal] with GRGM1200A to d/o=600.. Many features on these two maps are similar, further features and many details are missing in the upper figure; they are below the relevant resolution, of course. Sometimes, however, we can register artefacts – false waves which are removed when the “true” full field (d/o=600) is employed.

Now we can imagine what all with the solution to d/o=10 only would be lost, would remain hidden to us from the “real gravity world” of the Moon. Moreover, we can see that some false features would be created owing to the long-wavelengths (a form of aliasing). This might lead to various misinterpretations when we would have at our disposal only such a limited knowledge.

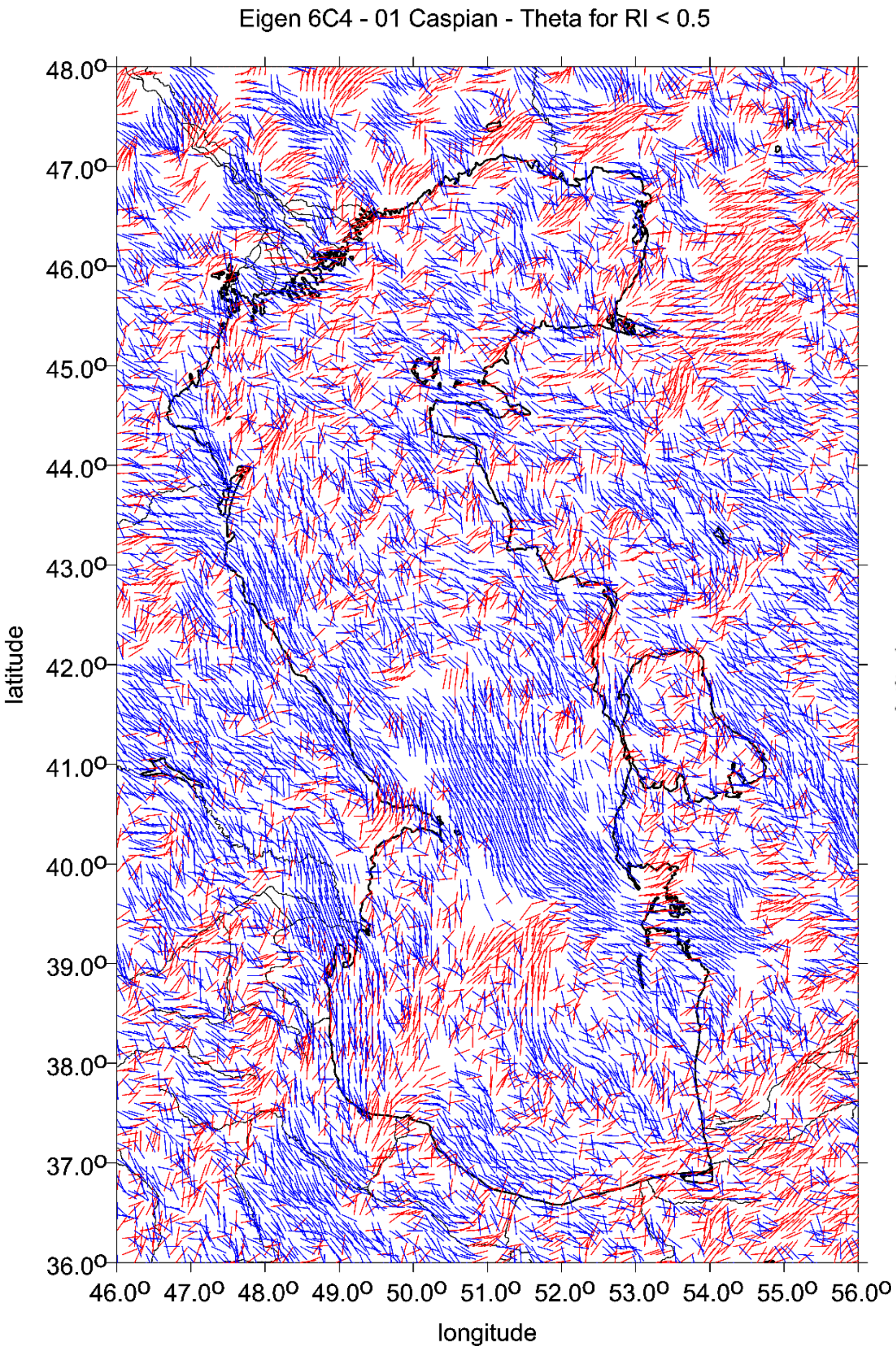

Eigen 6C4 - 01 Caspian - Theta for RI < 0.5
latitude
longitude
48.0°
47.0°
46.0°
45.0°
44.0°
43.0°
42.0°
41.0°
40.0°
39.0°
38.0°
37.0°
36.0°
46.0°
47.0°
48.0°
49.0°
50.0°
51.0°
52.0°
53.0°
54.0°
55.0°
56.0°

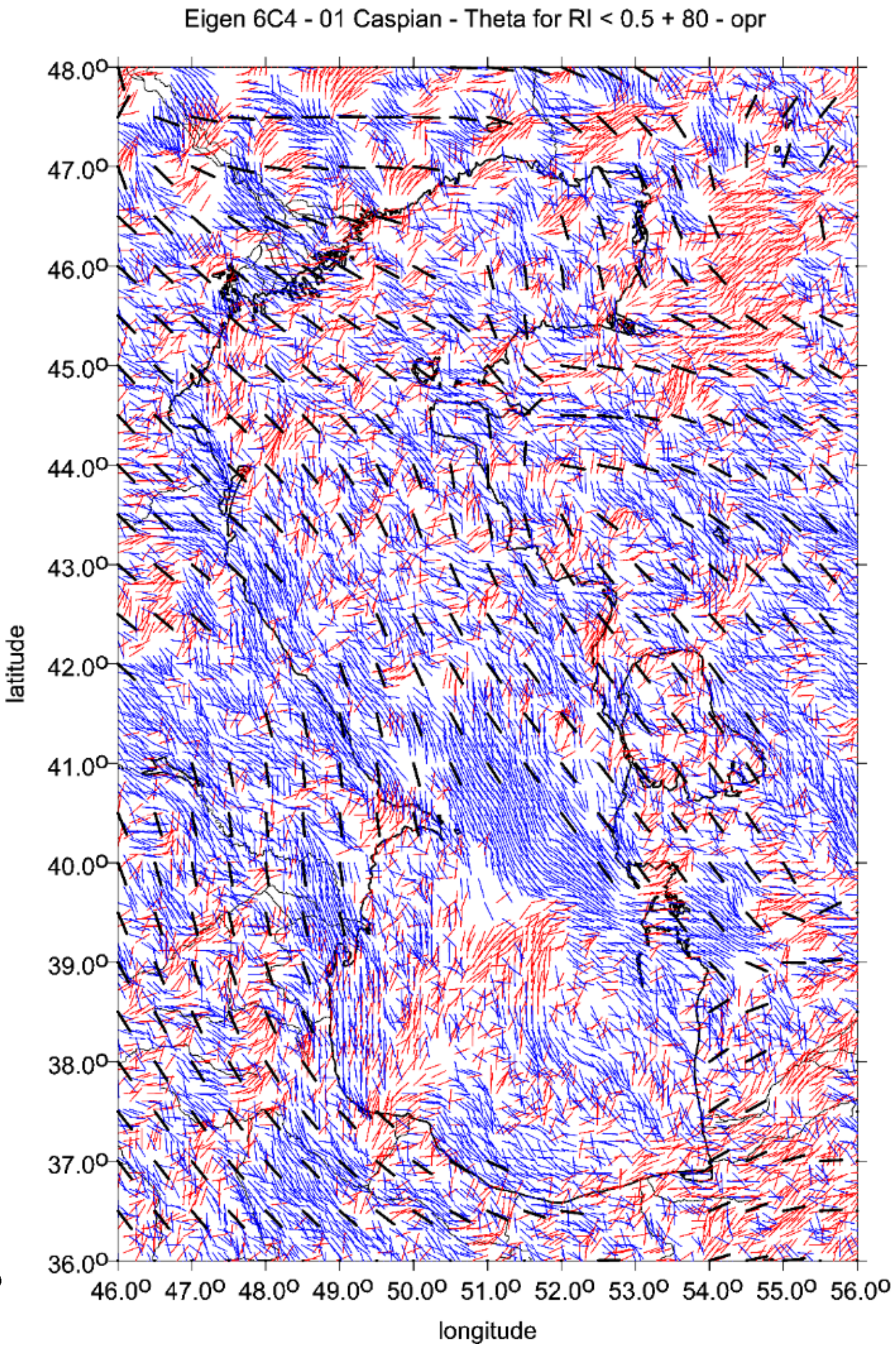

Eigen 6C4 - 01 Caspian - Theta for RI < 0.5 + 80 - opr
latitude
longitude
48.0°
47.0°
46.0°
45.0°
44.0°
43.0°
42.0°
41.0°
40.0°
39.0°
38.0°
37.0°
36.0°
46.0°
47.0°
48.0°
49.0°
50.0°
51.0°
52.0°
53.0°
54.0°
55.0°
56.0°

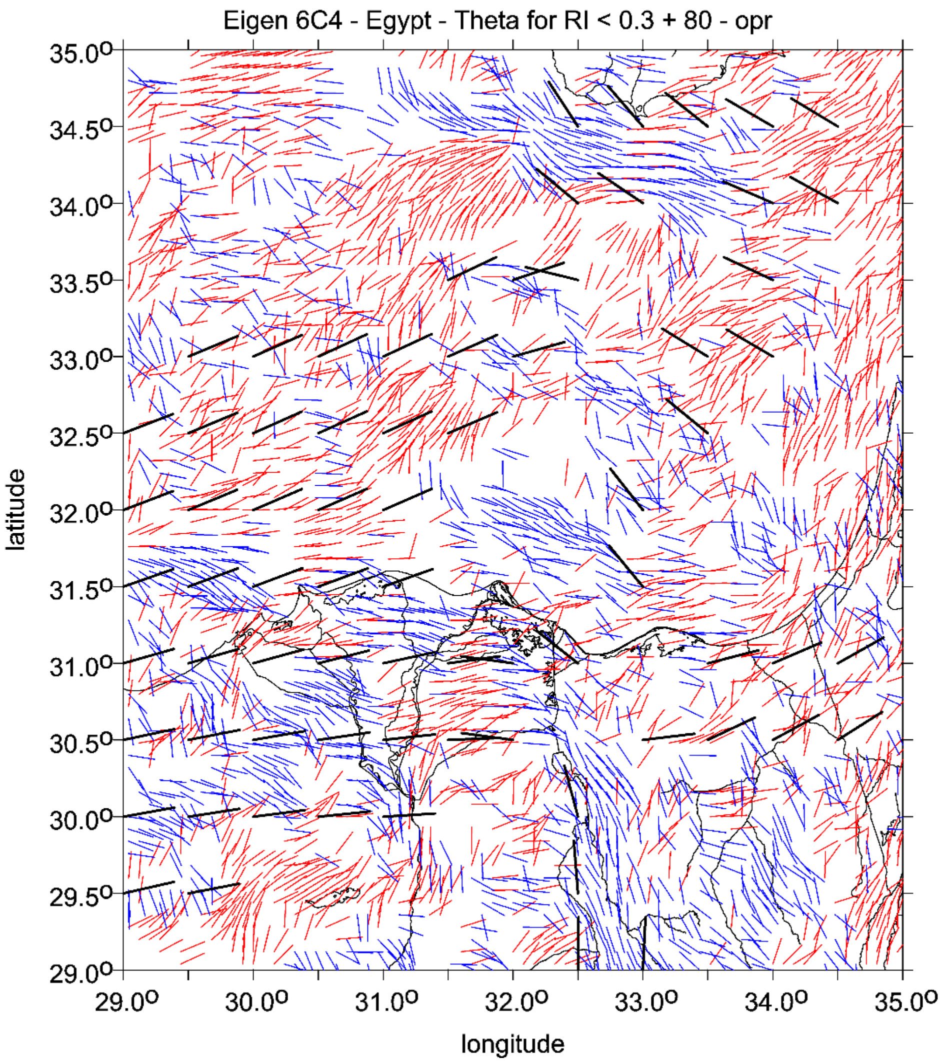
Eigen 6C4 - Egypt - Theta for RI < 0.3 + 80 - opr
latitude
longitude
35.0°
34.5°
34.0°
33.5°
33.0°
32.5°
32.0°
31.5°
31.0°
30.5°
30.0°
29.5°
29.0°
29.0°
30.0°
31.0°
32.0°
33.0°
34.0°
35.0°

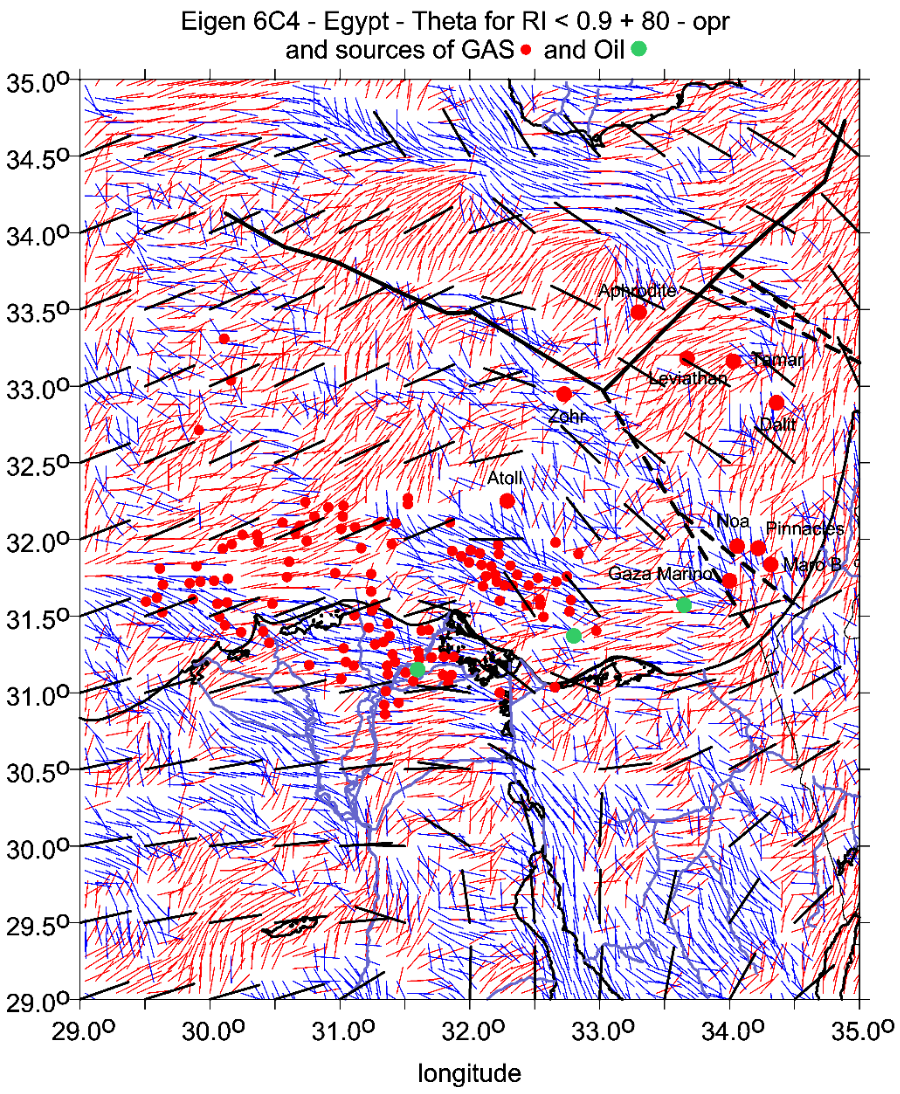
Eigen 6C4 - Egypt - Theta for RI < 0.9 + 80 - opr
and sources of GAS and Oil
Aphrodite
Tamar
Leviathan
Zohr
Dalit
Atoll
Noa
Pinnacles
Gaza Marino
Mari B
longitude
35.0°
34.5°
34.0°
33.5°
33.0°
32.5°
32.0°
31.5°
31.0°
30.5°
30.0°
29.5°
29.0°
29.0°
30.0°
31.0°
32.0°
33.0°
34.0°
35.0°

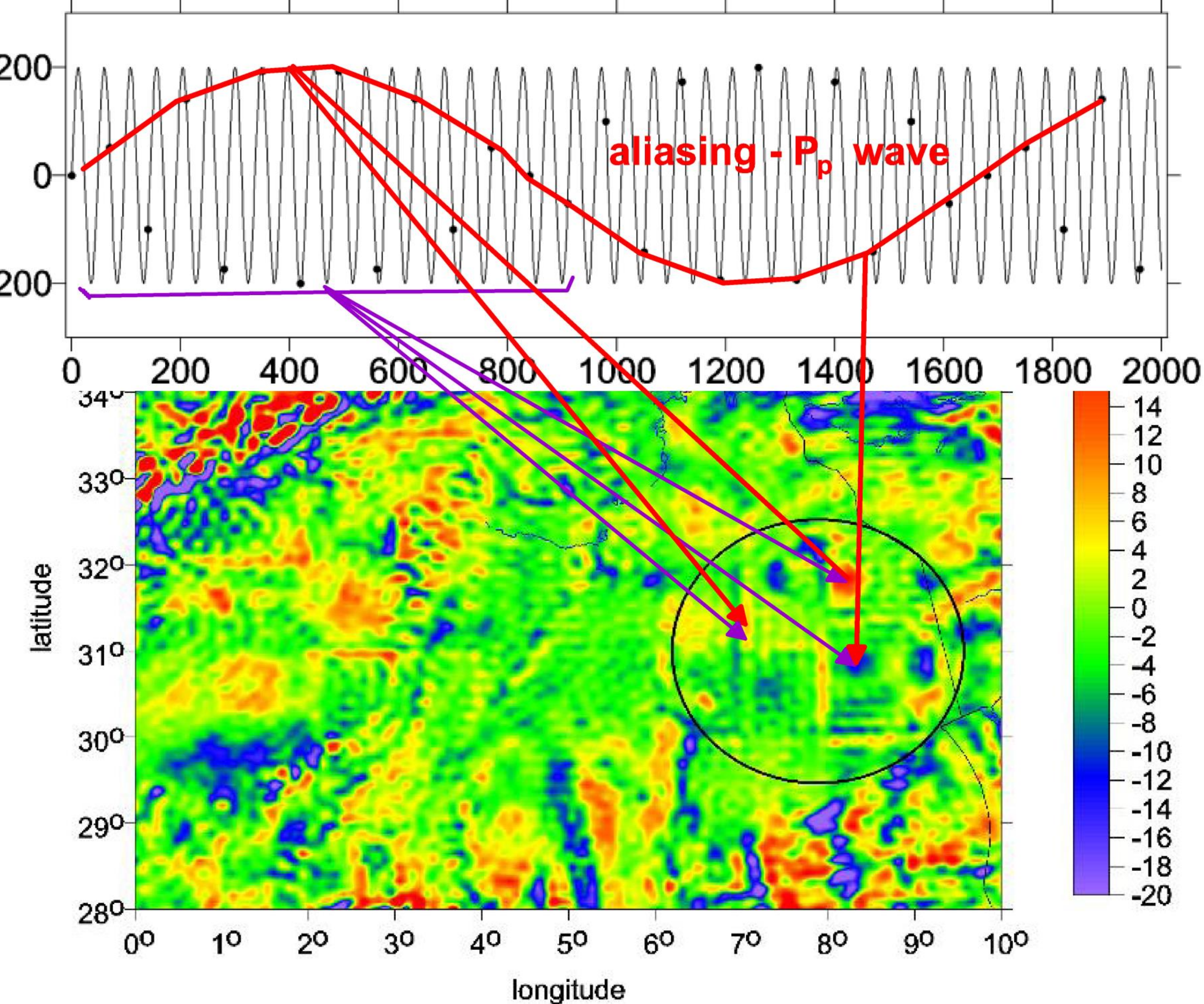

aliasing,
one type of the artefacts

the Earth, Sahara

Tunisia-Algeria,
the Chotts paleo-megalake.

Tzz [E] **with EIGEN6C4 to d/o=2190**

the peculiar artefacts in desert (encircled) and graining are discussed in Klokočník et al. (2021):

Chicxulub and Popigai on a globe

see Supplements 3 and 4

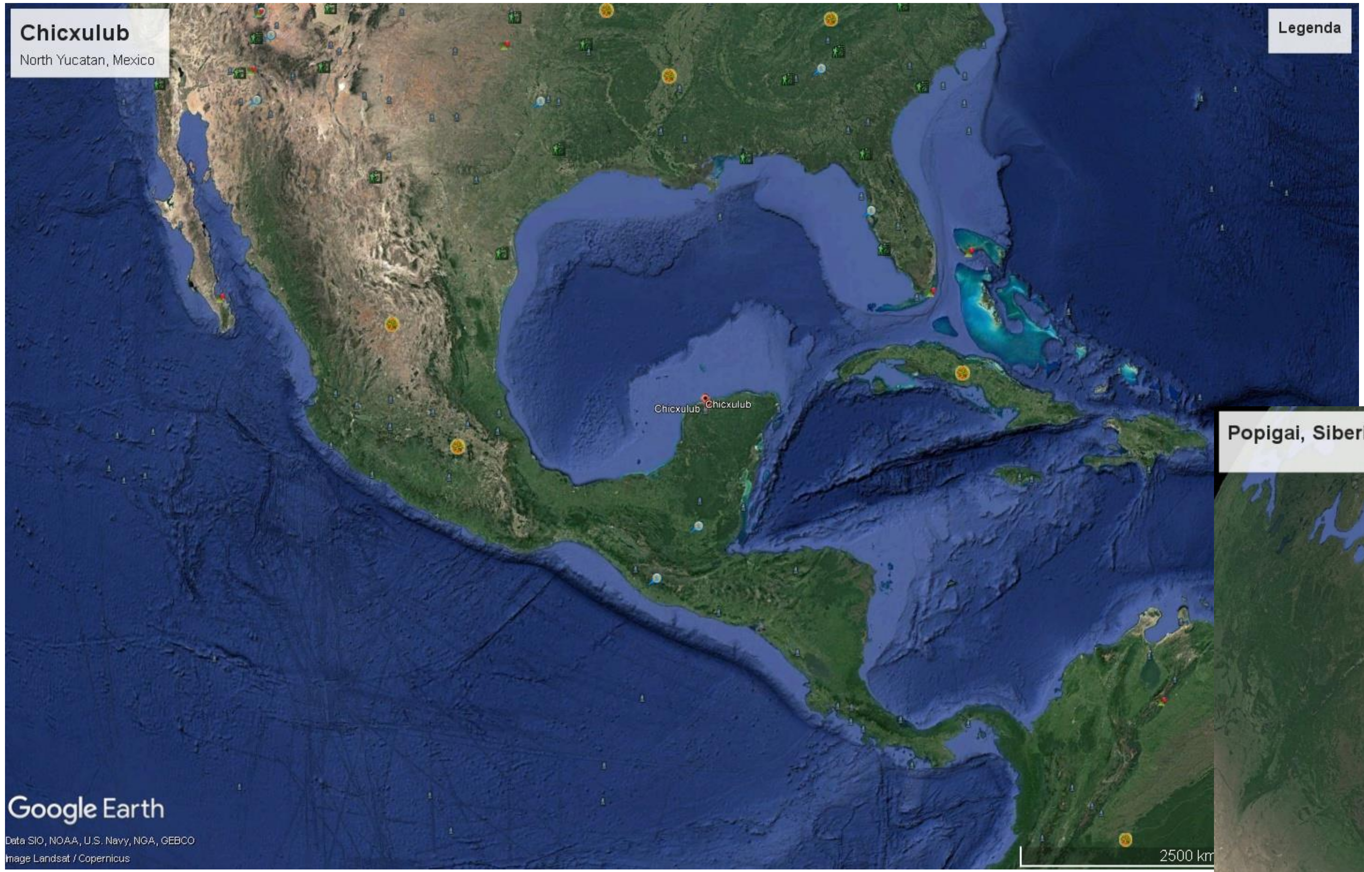

Astronomical Institute of the Czech Academy of Sciences

www/asu.cas.cz/~jklokocn
jklokocn@asu.cas.cz

The End of S2